Supplementary Materials

Contents

A. FILTERING

Preprocessing filter: The algorithm in the current study calculates features from filtered and unfiltered electrocardiogram (ECG) signals in parallel. Filtered ECGs were first preprocessed by applying a 1-30 Hz 4th order Butterworth bandpass filter with forwards-backwards implementation to reduce potential high-frequency noise (Figure 1, Figure 2).

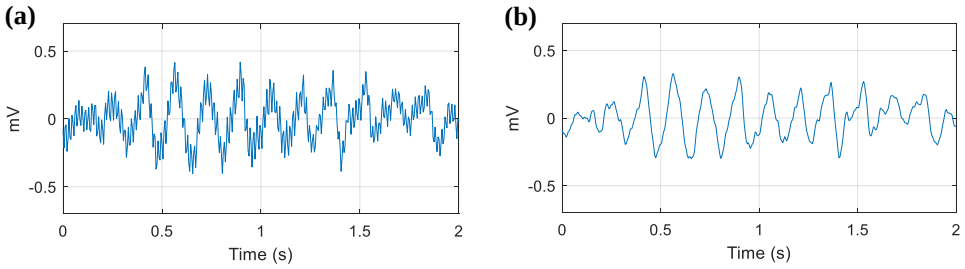

Figure 1. ECG powerline noise example
(a) Example of powerline noise in an unfiltered defibrillator ECG. (b) Low-pass-filtered ECG.

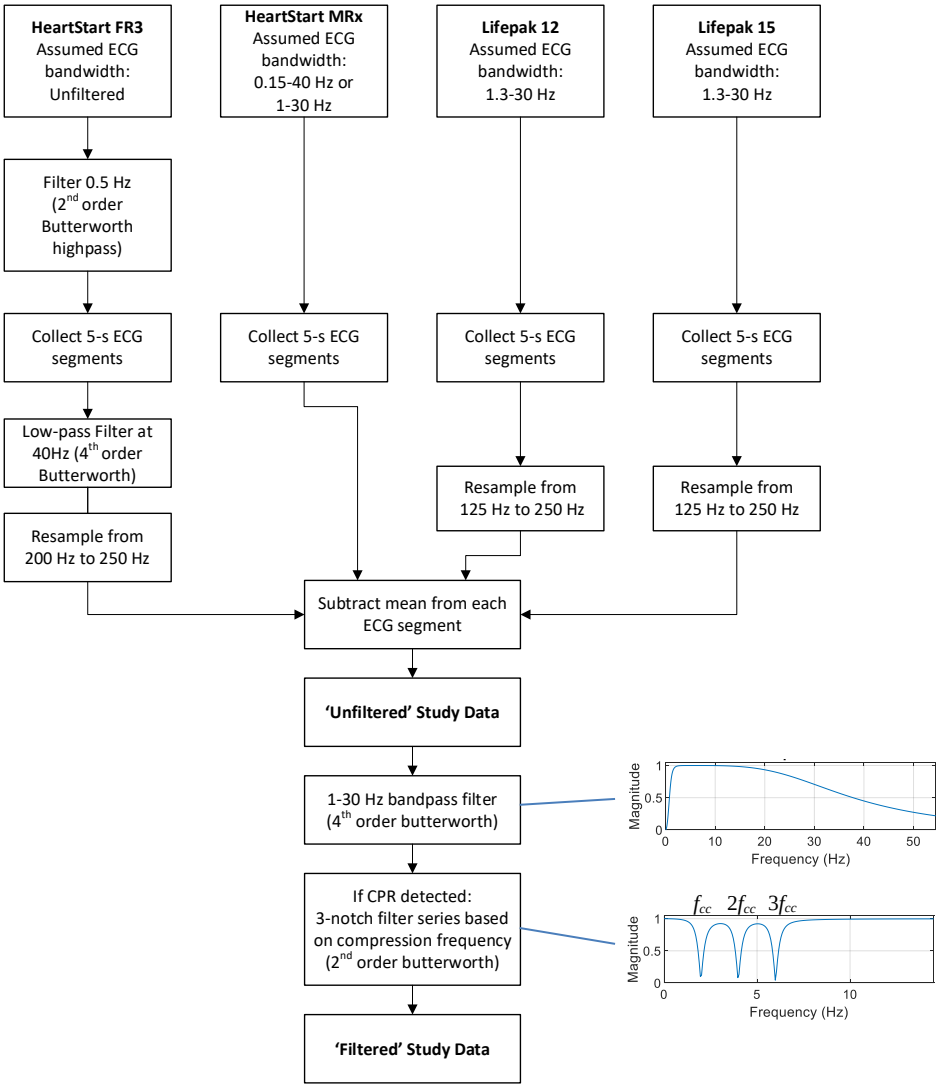

Figure 2. ECG data preprocessing and filtering

Notch filter: Following preprocessing, ECGs were processed with a notch filter to reduce chest compression artifact. To simulate real-world conditions during validation, the variable-frequency notch filter was only applied when compressions were automatically detected in the transthoracic impedance (TTI) signal using a TTI-based chest compression detection algorithm which we described previously.[1] Following the rationale of Gong et al. for implementation of filtering to reduce chest compression artifact, we implemented the variable-frequency notch filter based on

the estimated compression fundamental frequency f_{cc} in the TTI signal spectrum.[2] Deviating from the methods of Gong et al., once the presence of compressions was detected we then identified the estimated compression frequency f_{cc} as the frequency of the maximum peak within a predefined frequency range of the TTI spectrum. Although resuscitation guidelines dictate a target chest compression rate between 100-120 compressions per minute, rates can potentially vary more across individual rescuers.[3,4] Therefore, while prior methods have assumed a compression rate range of 60-210 compressions per minute, we assumed a range of 66–174 compressions per minute.[5] We then calculated f_{cc} as the frequency of the maximum peak in the TTI spectrum between 1.1–2.9 Hz. Then, as the frequency resolution in the ECG is greater than that of the TTI (by a factor of 2 to 4 depending on the device), f_{cc} was adjusted to match the frequency of the maximum peak in the ECG spectrum within a tolerance of +/- 0.3 Hz of the original f_{cc} estimated from the TTI spectrum. To apply the filter, a series of Butterworth notch filters was then applied to the ECG using forward-backwards implementation and centered at frequencies f_{cc}, $2f_{cc}$, and $3f_{cc}$ to remove the estimated fundamental and first two harmonic frequencies of compression artifact in the ECG (see manuscript Figure 3). Filter notch harmonic frequencies were based on multiples of the estimated compression fundamental rather than individually adjusted to compression harmonic peak frequencies observed in the ECG spectrum because VF rotor frequencies are typically centered at approximately 3-8 Hz and may overlap (and thus hinder precise detection of) the first and second chest compression harmonics.[6–9]

Filter parameters were selected empirically to maximize training AUC for predicting survival using a representative group of basic waveform metrics, with final notch bandwidth = 0.55 Hz, filter order = 2, and number of notches = 3.

Table 1. Selection of number of filter notches with training data and basic waveform metrics
Basic waveform measure AUC values for predicting patient outcomes on training data (460 patients) during chest compressions are presented. AUC values are compared using ECG segments filtered to remove the compression fundamental frequency (1 notch), the compression fundamental and first harmonic (2 notches), the compression fundamental and first two harmonics (3 notches), and the compression fundamental and first three harmonics (4 notches). Significance of AUC increase is calculated as p-value for difference versus AUC with no notch filtering. The configuration with 3 filter notches was selected as the final implementation. (AMSA = amplitude spectrum area, AUC = area under the receiver operating characteristic curve, RMS = root mean square.)

Outcome	Prognostic Metric	AUC with 4 Notches	AUC with 3 Notches	AUC with 2 Notches	AUC with 1 Notch	AUC with No Filter
Functional Survival	Peak Amplitude[10]	0.638*	0.645*	0.641*	0.628*	0.598
	RMS Amplitude[10]	0.648*	0.657*	0.647*	0.625*	0.583
	$AMSA_{1\text{-}26Hz}$[11,12]	0.707*	0.706*	0.702	0.702*	0.698
Defibrillation Success	Peak Amplitude[10]	0.624	0.635*	0.638*	0.630*	0.614
	RMS Amplitude[10]	0.638*	0.647*	0.645*	0.616*	0.590
	$AMSA_{1\text{-}26Hz}$[11,12]	0.667	0.668*	0.667*	0.664*	0.660

*p<0.05 versus AUC with no filter

B. ECG Amplitude Features with Parameter Selections

VF amplitude may be related to the size of depolarization waves in the ventricular myocardium and the number of cells contributing to any given wave, with higher VF amplitude generally associated with greater spatiotemporal organization and likelihood of defibrillation success. During VF, local areas in the myocardium depolarize synchronously in three-dimensional spiral and vortex waves, with the contractions becoming less coordinated over time as the functional units of contraction decrease in size and increase in number.[13–16] Thus early investigation by Weaver et al. demonstrated that higher-amplitude coarse VF (suggesting a relatively high amount of spatiotemporal organization) was associated with increased likelihood of conversion to organized rhythm following shock, while lower-amplitude fine VF (suggesting a relatively low amount of spatiotemporal organization) most often resulted in asystole when shocked.[10] However, prediction of outcome based on VF amplitude is confounded by voltage changes caused during

chest compressions, challenging potential integration of amplitude features in a prognostic algorithm designed to limit chest compression interruption.

In the current investigation, we designed two amplitude-based features of the VF signal. To improve performance and allow these features to resist the effects of transient chest compression artifact, we calculated the median of the amplitude in a sliding window to exclude spurious high-amplitude values. To allow the features to avoid low-frequency compression and ventilation artifact, we optimized window lengths to limit analysis to short periods within the signal (hence ignoring lower-frequency fluctuations). Specifically, the *Sliding Deviation* of VF ECG amplitude was calculated as

$$Sliding\ Deviation = \text{median}(s_{0,\ldots k\ldots,K}), \tag{1}$$

where

$$s_{0,\ldots k\ldots,K} = \sqrt{\frac{\sum_{n=k}^{k+W_{SD}-1}\left(|x_n| - \frac{1}{W_{SD}}\left(\sum_{n=k}^{k+W_{SD}-1}|x_n|\right)\right)^2}{W_{SD}-1}}, \tag{2}$$

W_{SD} is the window length (in samples), $x_0,\ldots,x_n,\ldots,x_{N-1}$ are N zero-mean ECG voltage samples collected during 5 seconds of VF, and $K = N - W_{SD} - 1$. Similarly, we calculated the *Sliding Peak* amplitude as

$$Sliding\ Peak = \text{median}(p_{0,\ldots k\ldots,K}), \tag{3}$$

where

$$p_{0,\ldots k\ldots,K} = \max|x_n|,\ \ \{n \mid k \le n < k + W_{SP}\}, \tag{4}$$

W_{SP} is the window length, and $K = N - W_{SP} - 1$ (Figure 3).

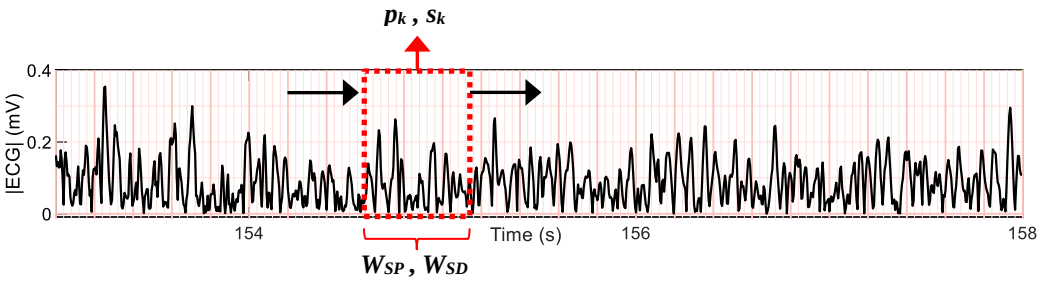

Figure 3. Amplitude-based ECG features
Median of standard deviation and peak amplitudes are calculated from the absolute-value ECG within sliding variable-length windows for both *Sliding Deviation* and *Sliding Peak*.

We selected W_{SD} and W_{SP} to maximize training AUC for predicting survival and return of rhythm. Optimizations were performed with and without compressions and for filtered and unfiltered ECG segments separately (Figure 4, Figure 5).

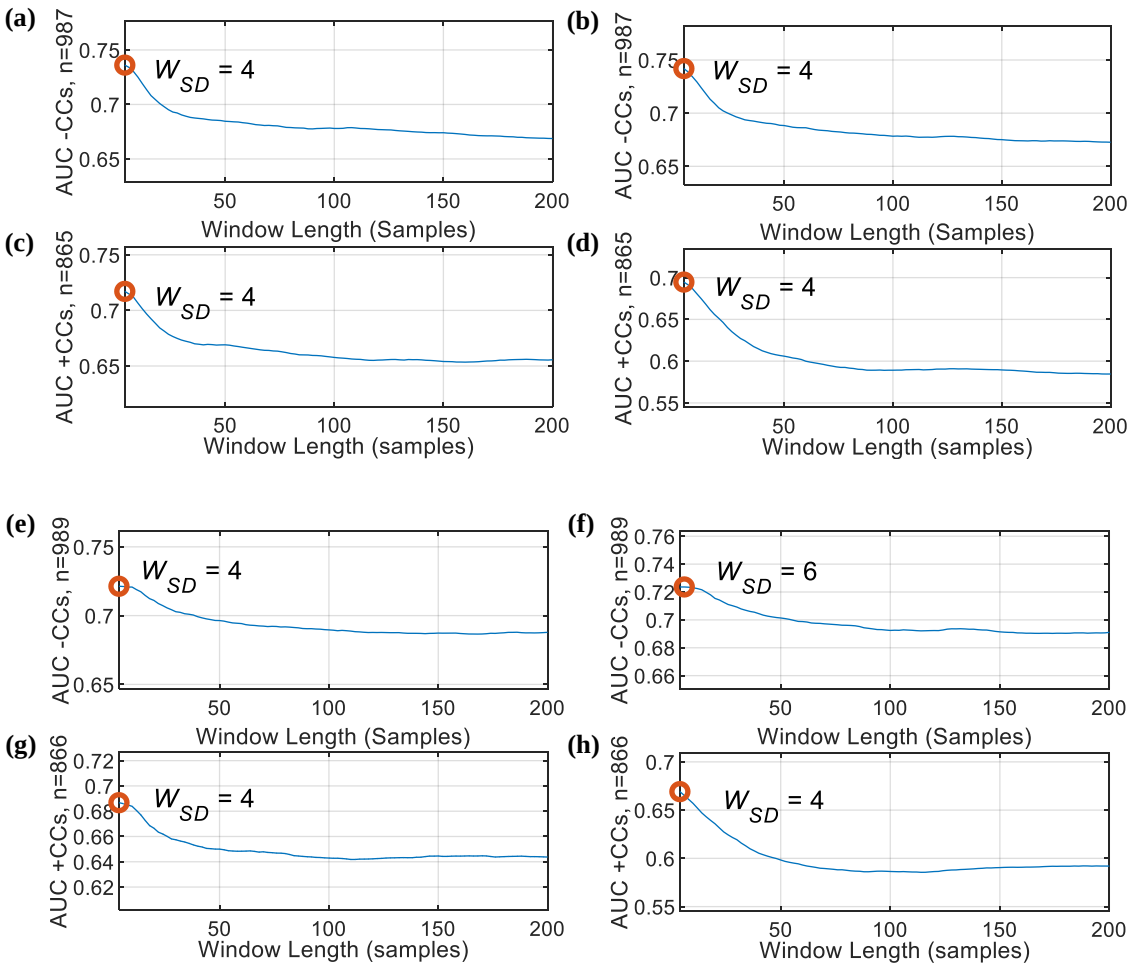

Figure 4. ***Sliding Deviation*** **parameter selection**
Parameter selections for W_{SD} based on training data for prediction of (a) survival -CCs, (b) survival -CCs using unfiltered data, (c) survival +CCs, (d) survival +CCs using unfiltered data, (e) return of rhythm -CCs, (f) return of rhythm -CCs using unfiltered data, (g) return of rhythm +CCs, (h) return of rhythm +CCs using unfiltered data. Minimum allowable x-value is W = 4 samples. (-CCs = without chest compressions, +CCs = with chest compressions.)

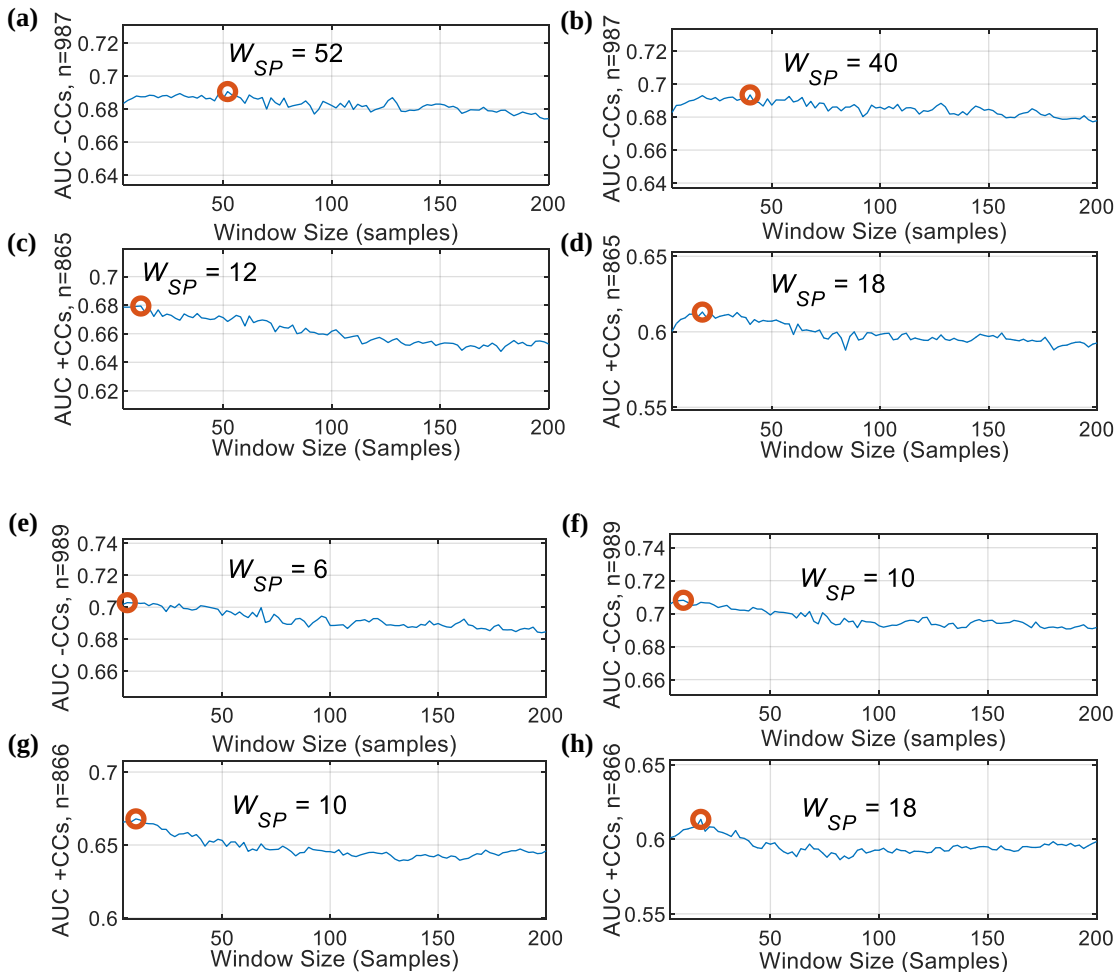

Figure 5. *Sliding Peak* parameter selection
Parameter selections for W_{SP} based on training data for prediction of (a) survival -CCs, (b) survival -CCs using unfiltered data, (c) survival +CCs, (d) survival +CCs using unfiltered data, (e) return of rhythm -CCs, (f) return of rhythm -CCs using unfiltered data, (g) return of rhythm +CCs, (h) return of rhythm +CCs using unfiltered data. Minimum allowable x-value is W = 4 samples. (-CCs = without chest compressions, +CCs = with chest compressions.)

C. ECG Time-Frequency Entropy and Energy Features with Parameter Selections

The complex Morlet wavelet $\psi(t)$ can be described as a sinusoid with a Gaussian envelope; i.e., $\psi(t) = \pi^{-1/4} \exp(\mathrm{i}2\pi f_0 t) \exp(-t^2/2)$, given time t and base frequency $f_0 = \sqrt{1/(2\ln 2)}$.[17] The mother wavelet $\psi(t)$ can be scaled to specific center frequencies using a scale factor, a, and

computing $\psi(t/a)$. Convolving an input signal $x_0,...,x_n,...,x_{N-1}$ and a wavelet with known center frequency in discrete time therefore has an effect similar to a bandpass filter, producing output coefficients w_n, where index n in the wavelet coefficient output vector corresponds to the sampling index n of the input x (after truncation following convolution to align the two signals). Multiple wavelets with known center frequencies f_j (with j indicating frequency index and f typically spaced logarithmically in Hz) can be convolved with an input x to produce a matrix of values $|w_{n,j}|$ at sampling indices n and frequency indices j to construct a scalogram of x (Figure 6). Such wavelet-based time-frequency transforms are considered to have superior temporal resolution compared to traditional time-frequency methods such as the short-time Fourier transform.[18]

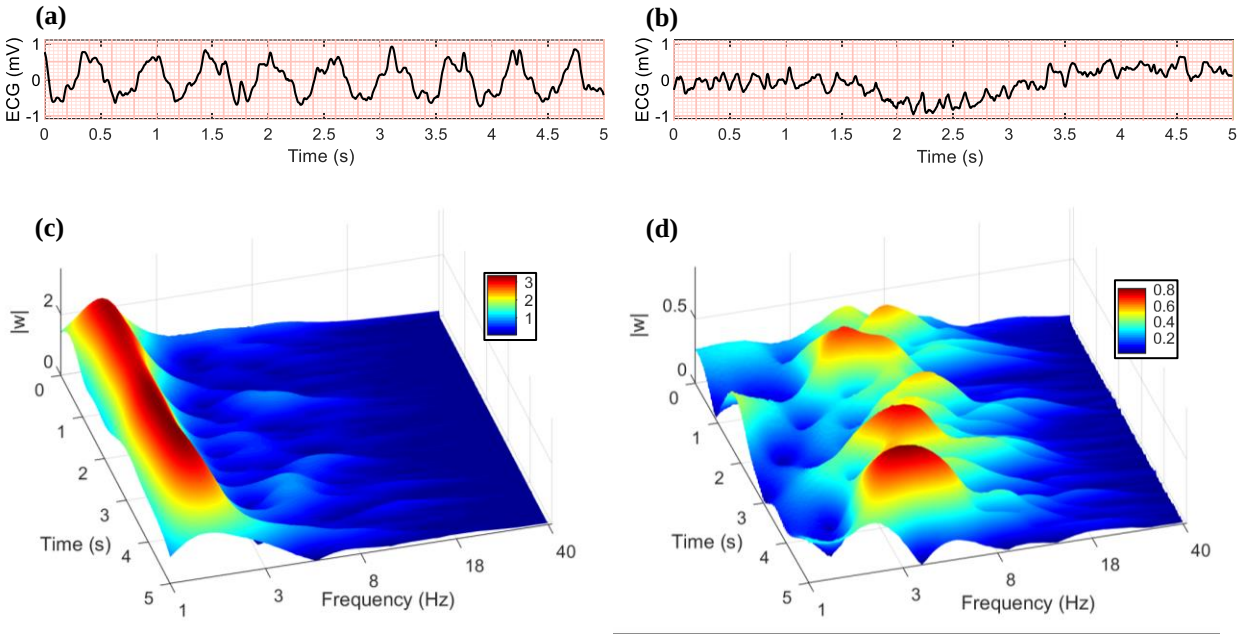

Figure 6. Wavelet scalograms of VF with and without CPR
Example of VF segments collected adjacent to each other prior to the same shock with compressions (a) and without compressions (b). Compression artifact is visible in (a) as large oscillations in the ECG which obscure the VF, and the low-frequency drift in (b) is due to an artificial respiration. Scalograms are shown for the VF with compressions in (c) and without compressions in (d).

Prior investigations have demonstrated methods to predict defibrillation outcomes by designing features derived from wavelet transforms of the VF ECG.[17,19–22] These investigations were limited to analysis without chest compression artifact. In subsequent investigation, we demonstrated that during chest compressions, high-frequency energy in the wavelet transform as described by Endoh et al. exhibited superior performance during chest compressions as compared to other individual features of the VF waveform.[22,23] However, simply computing the total energy within a defined frequency range of the wavelet transform (as in Endoh et al.) ignores time-dependent behavior that could otherwise be exploited. Hence, in the current investigation we sought to design features of the VF wavelet transform that describe time-variant and frequency-

variant properties of the wavelet transform, and to incorporate variable parameters in such a way to allow ECG features to ignore chest compression artifact.

Shannon originally described a measurement of entropy that can be used to quantify the presence of unpredictable values and estimate information content.[24] Forms of the Shannon Entropy, $-\sum P_x \log_2 P_x$ (for P_x = probability of discrete value of x), have been applied to analysis of a variety of time-domain biological signals (such as electroencephalograms) as well as to analysis of these signals' Fourier and wavelet transforms.[25,26] An example applied to distributions of arbitrary signals is shown in Figure 7. With regards to prediction of defibrillation success, entropy-based features have been primarily been calculated directly from the time-domain ECG.[22,27–31] Entropy-like features to predict defibrillation outcome have also been calculated from wavelet transforms of the VF ECG. Specifically, Shandilya et al. calculated Shannon entropies within multiple frequencies of the wavelet scalogram, while Watson et al. calculated an entropy feature from a single frequency in the wavelet scalogram.[18,32–34] However, these prior studies have not calculated entropy features during chest compressions, and it was previously unknown whether the presence of compression artifact would confound entropy methods.

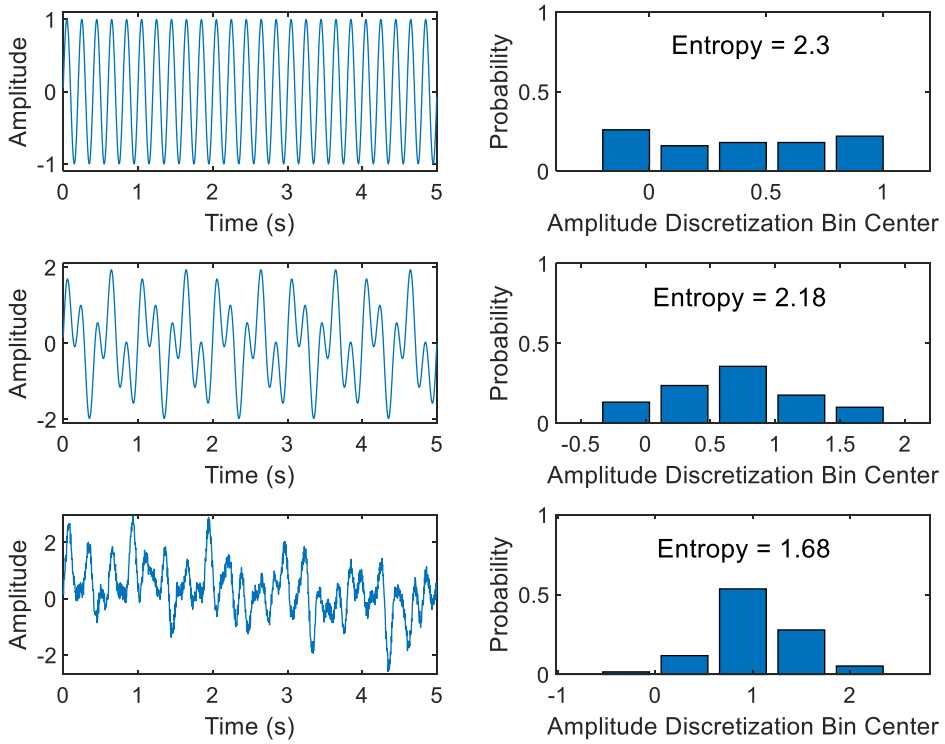

Figure 7 Arbitrary Shannon Entropy examples
Synthesized arbitrary sinusoidal signals with increasing numbers of sinusoids and noise (left) and the corresponding entropy values calculated from their probability distributions discretized into 5 bins (right). Signals with a flat distribution of values have higher entropy.

In the current investigation, we designed four features of the VF ECG related to likelihood of positive shock outcome using the Shannon equation to describe characteristics of the magnitude VF wavelet transform coefficients $|w_{n,j}|$. We designed the *Interfrequency Entropy* to quantify the time-varying spectral distribution as it evolves over the length of the VF segment. In contrast to prior wavelet-based entropy methods,[32,33] we calculated *Interfrequency Entropy* as the median of entropy values at each timepoint of the scalogram using variable magnitude probability bin resolutions and variable low frequency cutoffs. Specifically,

$$Interfrequency\ Entropy = \text{median}(h_{0,\ldots n,\ldots N-1}), \tag{5}$$

where

$$h_{0,\ldots n,\ldots .N-1} = -\sum_{b=1}^{B} P_{n,b}\left(\log_2 P_{n,b}\right), \tag{6}$$

P_n is the probability distribution of the magnitude wavelet coefficients $\left|w_{n,j}\right|$ at sample index n between frequency indices $j_{low} \le j \le j_{hi}$ (corresponding to the frequency range $[f_{low}, f_{hi}]$ in Hz), B is the number of discretizations (bins) in the probability distribution, b is the probability bin index, and N is the sample length of the original ECG input (Figure 8). While increased h in *Interfrequency Entropy* is associated with positive outcomes when applied across a wide frequency range, we also observed that analysis limited to high frequency content (i.e. above approximately 10 Hz) counterintuitively results in low h being associated with positive outcomes. Therefore, to describe the distribution of high-frequency content at each timepoint in the scalogram, we also calculated the *High-Frequency Entropy* as the inverse of the median of h, or

$$\textit{High-Frequency Entropy} = -\text{median}(h_{0,\ldots n,\ldots .N-1}), \tag{7}$$

where similarly,

$$h_{0,\ldots n,\ldots .N-1} = -\sum_{b=1}^{B} P_{n,b}\left(\log_2 P_{n,b}\right). \tag{8}$$

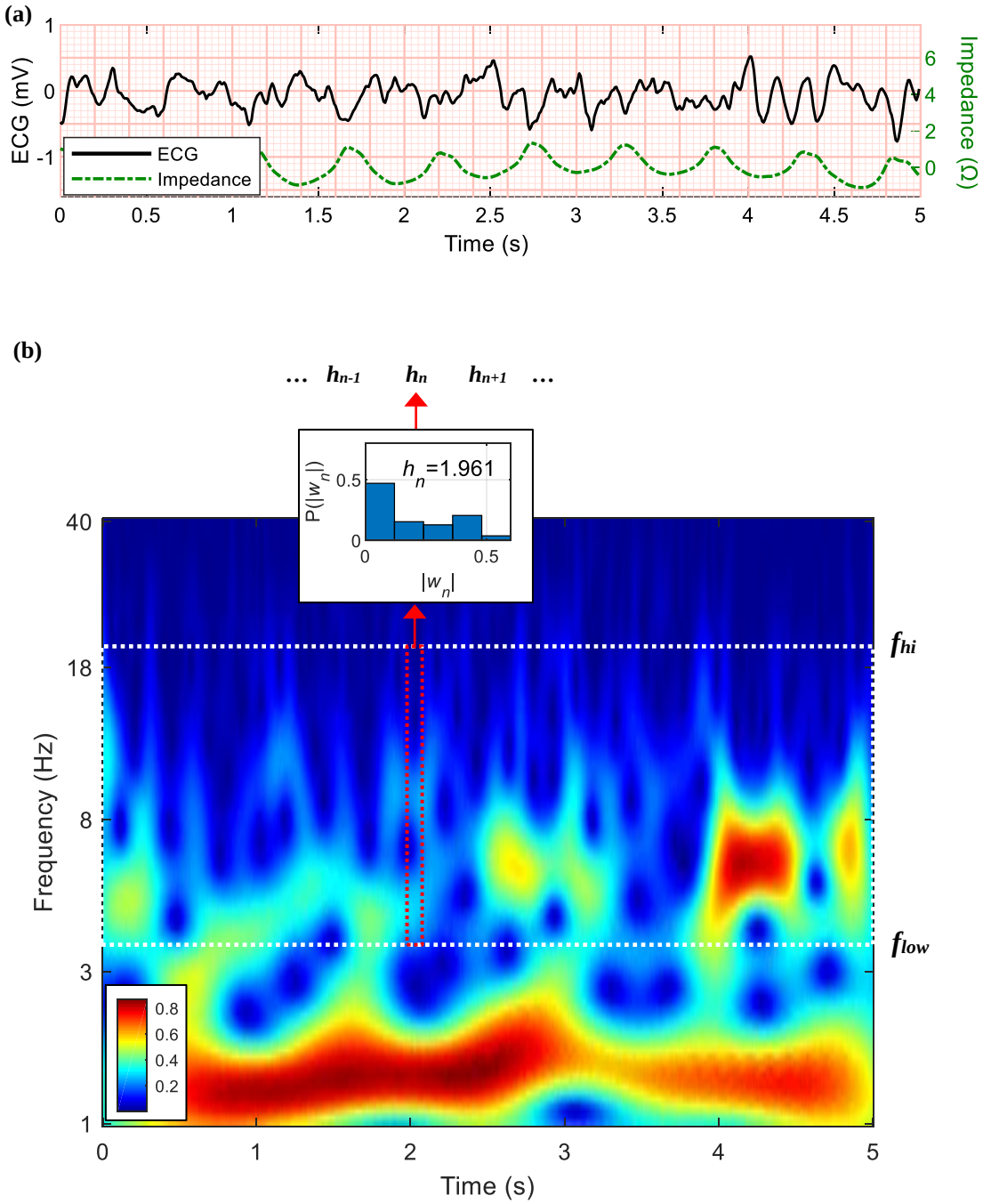

Figure 8. ***Interfrequency Entropy*** **and** ***High-Frequency Entropy***
(a) VF ECG during compressions with compressions confirmed in the impedance. (b) Scalogram of VF during compressions with compression fundamental band visible at approximately 1.5 Hz. To calculate entropy features, the scalogram is evaluated between variable frequency limits f_{low}-f_{hi} to calculate probability distributions P_n and generate h_n at for sample index. In this illustration, f_{low} is indicated at 3 Hz, which ignores the chest compression fundamental band below f_{low}.

Shannon-like entropy functions describe probability distributions normalized to a total area of 1 by definition; thus, information related to the overall amplitude of original signal is lost. For instance, *Interfrequency Entropy* above is calculated from the distribution of wavelet coefficient magnitudes within a range of frequencies at each timepoint, but the probability distribution of the coefficient magnitudes is normalized such that the absolute scale of the values are not accounted for (e.g., as in Figure 7, the actual x-values in the distributions are not used to calculate h). As we demonstrated in prior investigation after expanding on the methods of Endoh et al., however, the total energy in specific frequency ranges of the wavelet transform (particularly in higher frequencies) is strongly related to patient outcome during ongoing chest compressions and may offer additional information useful in conjunction with entropy.[22,23] Therefore, deviating from the methods of Endoh et al. which calculate the integral of scalogram magnitudes within fixed frequency ranges, we applied the Shannon entropy equation directly to the scalogram magnitude values in both the time and frequency directions within variable frequency ranges. Specifically, we calculated the *Shannon Energy* to describe the energy content at each frequency index j across all time indices n, and the *Interfrequency Shannon Energy* to describe the energy content within each time sample n in the scalogram across all frequency indices j. We applied the median operation in *Shannon Energy* to allow the function to ignore outliers in frequency caused by noise that may occur within narrow frequency ranges (such as regular compressions or other persistent noise). We applied the median operation in *Interfrequency Shannon Energy* to allow the function to ignore transient artifact outliers in time (such as severe individual compressions or transient motion artifact). We defined the *Shannon Energy* as

$$Shannon\ Energy = \text{median}(g^{SE}{}_{j_{low},\ldots j,\ldots j_{hi}}), \tag{9}$$

where

$$g^{SE}{}_{j_{low},\ldots j,\ldots j_{hi}} = -\sum_{n=0}^{N-1} \left| w_{n,j} \right| \left(\log_2 \left| w_{n,j} \right| \right), \tag{10}$$

$w_{n,j}$ are the wavelet coefficients at frequency indices j and time sample indices n, j_{low} and j_{hi} are the low and high frequency index limits corresponding to an analysis frequency range (in Hz) [f_{low} , f_{hi}], and N is the number of n time samples in the wavelet transform coefficients $w_{n,j}$ (Figure 9). We also calculated the *Interfrequency Shannon Energy* as

$$\textit{Interfrequency Shannon Energy} = \text{median}(g^{ISE}{}_{0,\ldots n,\ldots N-1}), \tag{11}$$

where

$$g^{ISE}{}_{0,\ldots n,\ldots N-1} = -\sum_{j=j_{low}}^{j_{hi}} \left| w_{n,j} \right| \left(\log_2 \left| w_{n,j} \right| \right). \tag{12}$$

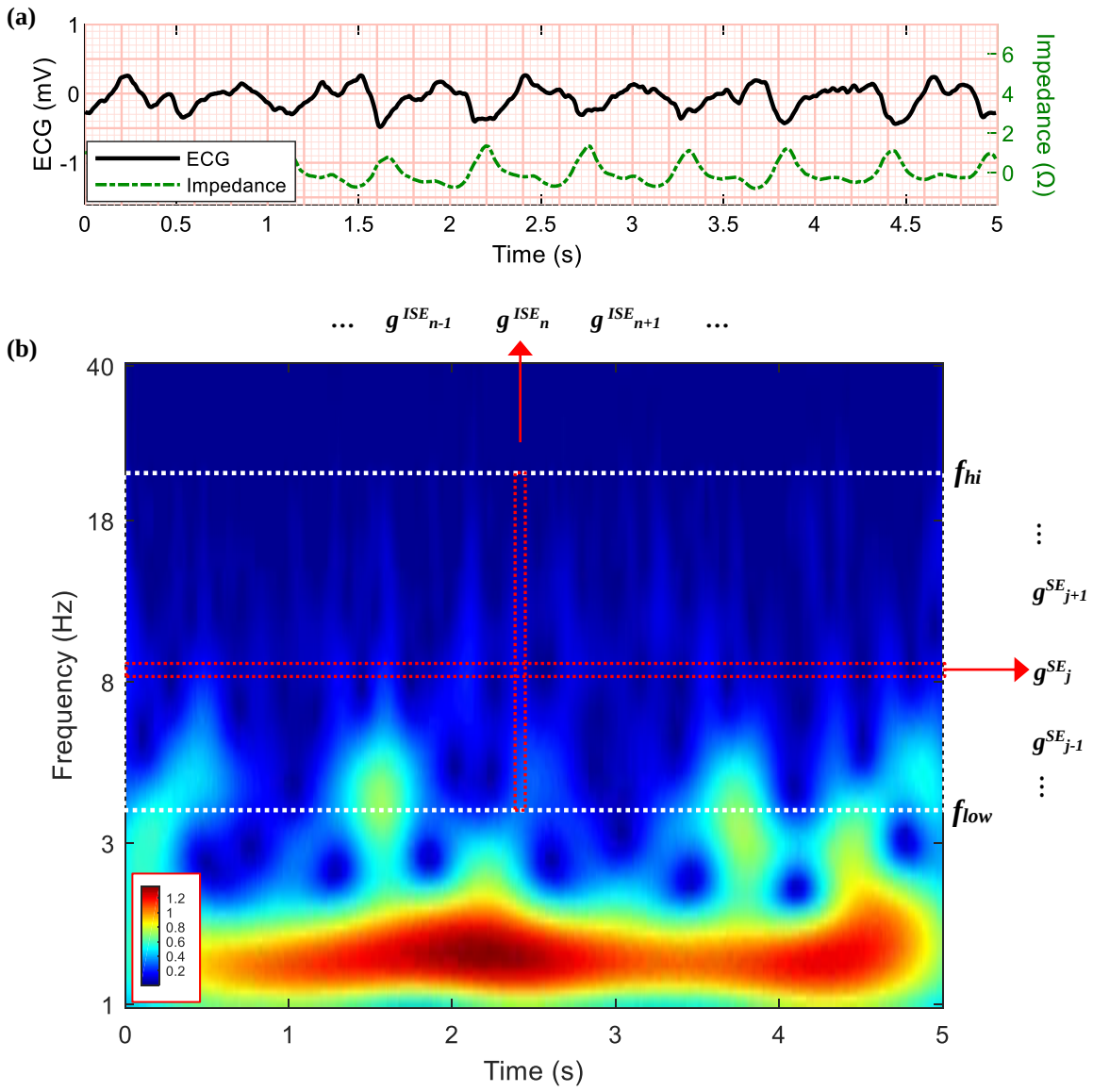

Figure 9. ***Shannon Energy*** **and** ***Interfrequency Shannon Energy***
(a) VF ECG during compressions, with compressions confirmed in the impedance. (b) Scalogram of VF during compressions with the compression fundamental band visible at approximately 1.5 Hz. To calculate features, the scalogram is evaluated between variable frequency limits f_{low}-f_{hi} to calculate *Shannon Energy* as the median of g^{SE} at each frequency and the *Interfrequency Shannon Energy* as the median of g^{ISE} at each time sample.

We optimized parameters in the four entropy-like functions described above to maximize performance with and without chest compressions using training data. To optimize *Interfrequency Entropy* and *High-Frequency Entropy*, we varied the low frequency limits of analysis and the

number of bins in the probability distributions used to calculate entropy. Specifically, in order to allow an inherent avoidance of low-frequency chest compression artifact, we varied the lowest frequency limit f_{low} (in Hz) corresponding to low frequency limit index j_{low}, and ignored frequencies in the wavelet transform below this threshold. The high frequency limit f_{hi} was set equal to the upper bandwidth limit of the signal (f_{hi} = 30 Hz for filtered data and f_{hi} = 40 Hz for unfiltered data). Furthermore, while the number of probability bins used to calculate ECG entropy has typically been chosen arbitrarily in prior investigations (e.g. on the order of 10—30 bins), we varied the number of discretization bins B to determine optimal bin resolutions.[26,27,33] To improve ability of the function to generalize, we simplified the function by limiting the maximum B to a value of eight. In contrast to *Interfrequency Entropy* and *High-Frequency Entropy*, the *Shannon Energy* and *Interfrequency Shannon Energy* are calculated directly from the wavelet transform coefficients and do not employ probability distributions; thus, for these functions, we varied both the low and high frequency limits defining the range of analysis $[f_{low}, f_{hi}]$ to determine the optimal corresponding frequency index limits j_{low} and j_{hi} to evaluate these functions. Varying both upper and lower frequency limits allowed these functions to avoid potential high-frequency noise and to reduce the effect of low-frequency compression artifact. Parameter optimizations for all four Shannon-based wavelet features are shown below in Figure 10 – Figure 13. Parameters were selected to maximize training AUC. Additionally, when optimizing both $[f_{low}, f_{hi}]$, the widest frequency range corresponding to an AUC within +/- 0.005 of the maximum AUC was selected to prevent overfitting to local maxima in the AUC optimization surface.

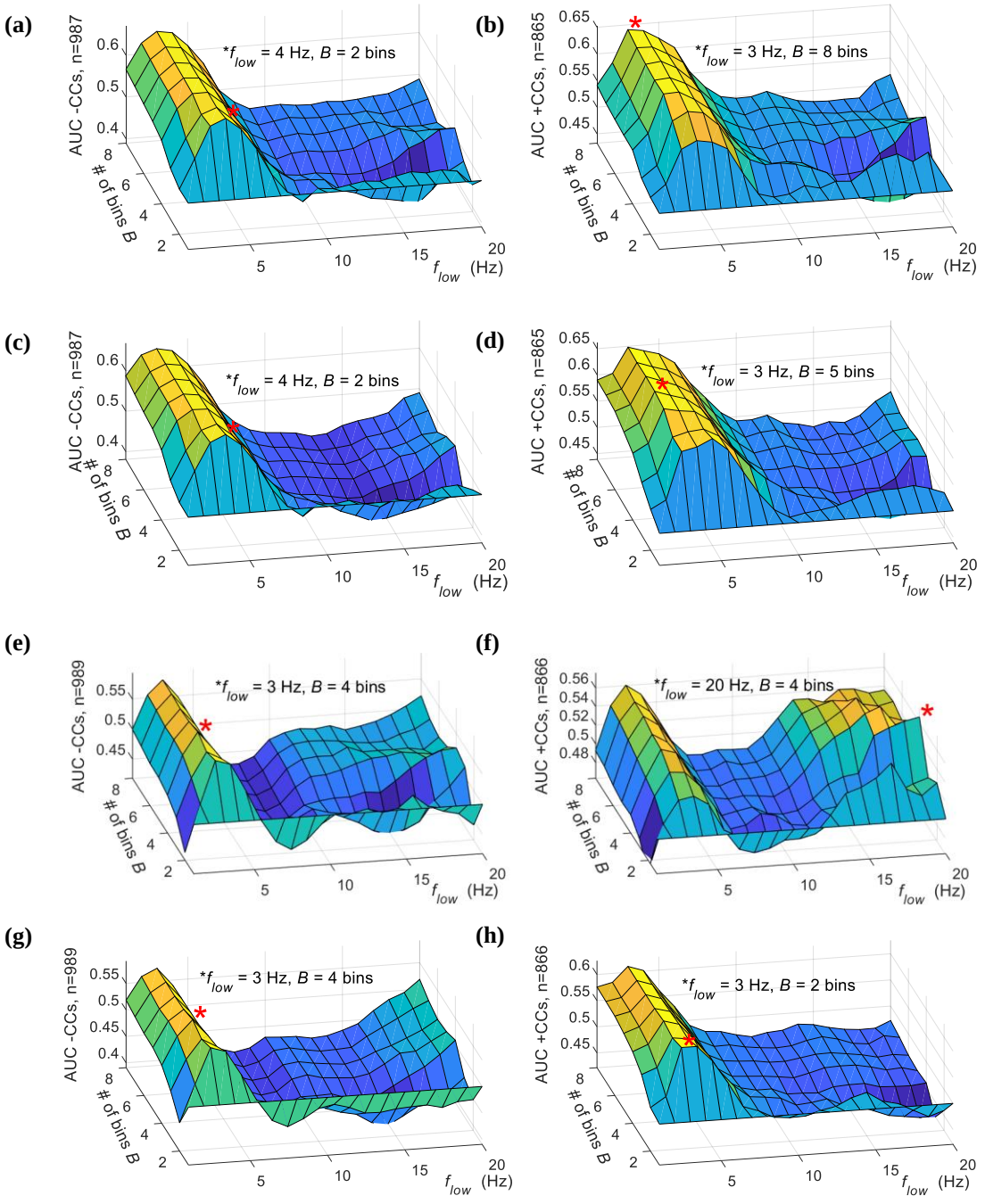

Figure 10. ***Interfrequency Entropy*** **parameter selection**
Parameter selections based on training data area under the receiver operating characteristic curve (AUC) for *Interfrequency Entropy* for predicting survival using filtered data (a) without compressions (-CCs) and (b) with compressions (+CCs), for predicting survival using unfiltered data (c) -CCs and (d) +CCs, for predicting return of rhythm using filtered data (e) -CCs and (f) +CCs, and for predicting return of rhythm using unfiltered data (g) -CCs and (h) +CCs.

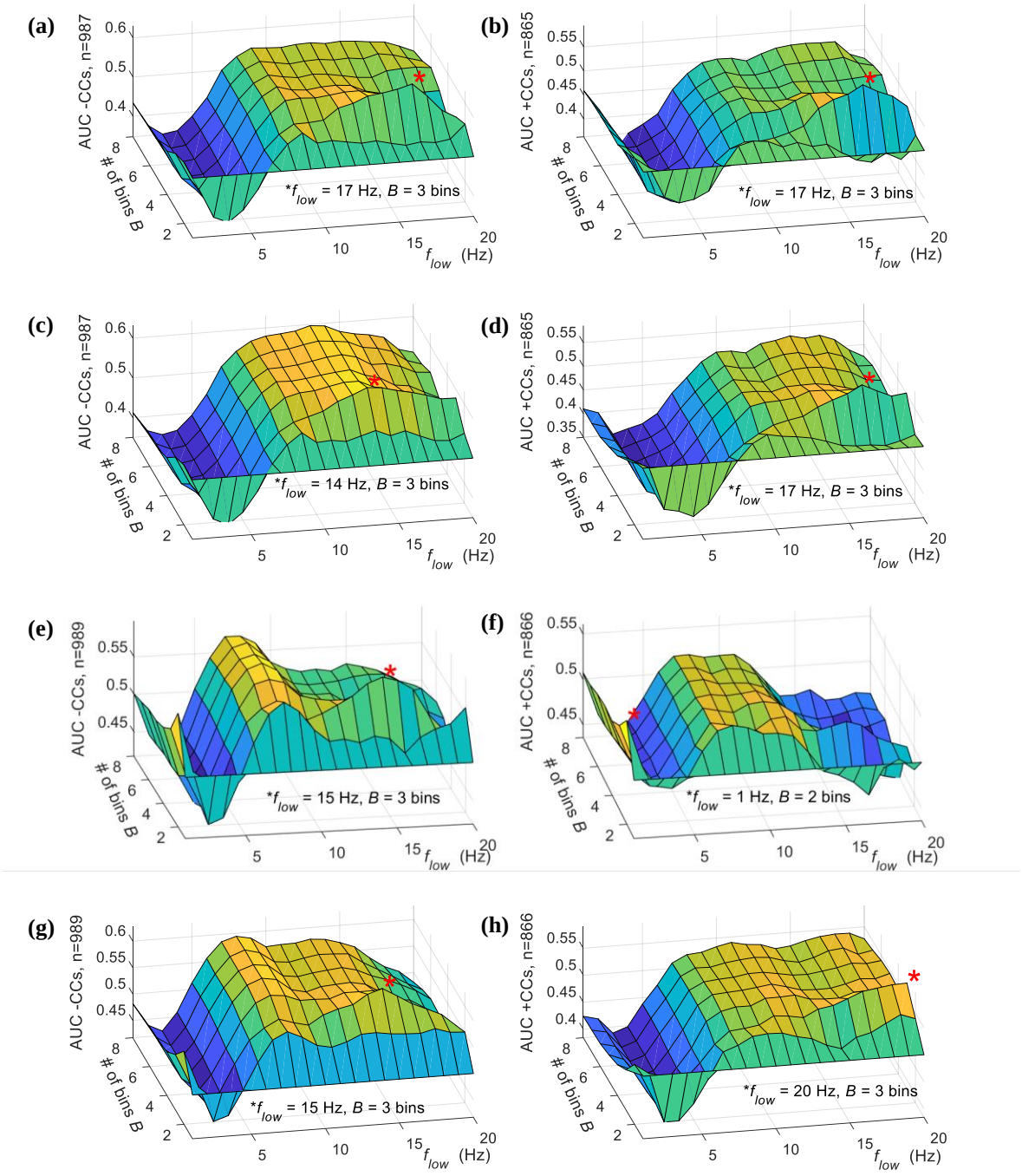

Figure 11. *High-Frequency Entropy* parameter selection
Parameter selections based on training data area under the receiver operating characteristic curve (AUC) for *High-Frequency Entropy* for predicting survival using filtered data (a) without compressions (-CCs) and (b) with compressions (+CCs), for predicting survival using unfiltered data (c) -CCs and (d) +CCs, for predicting return of rhythm using filtered data (e) -CCs and (f) +CCs, and for predicting return of rhythm using unfiltered data (g) -CCs and (h) +CCs.

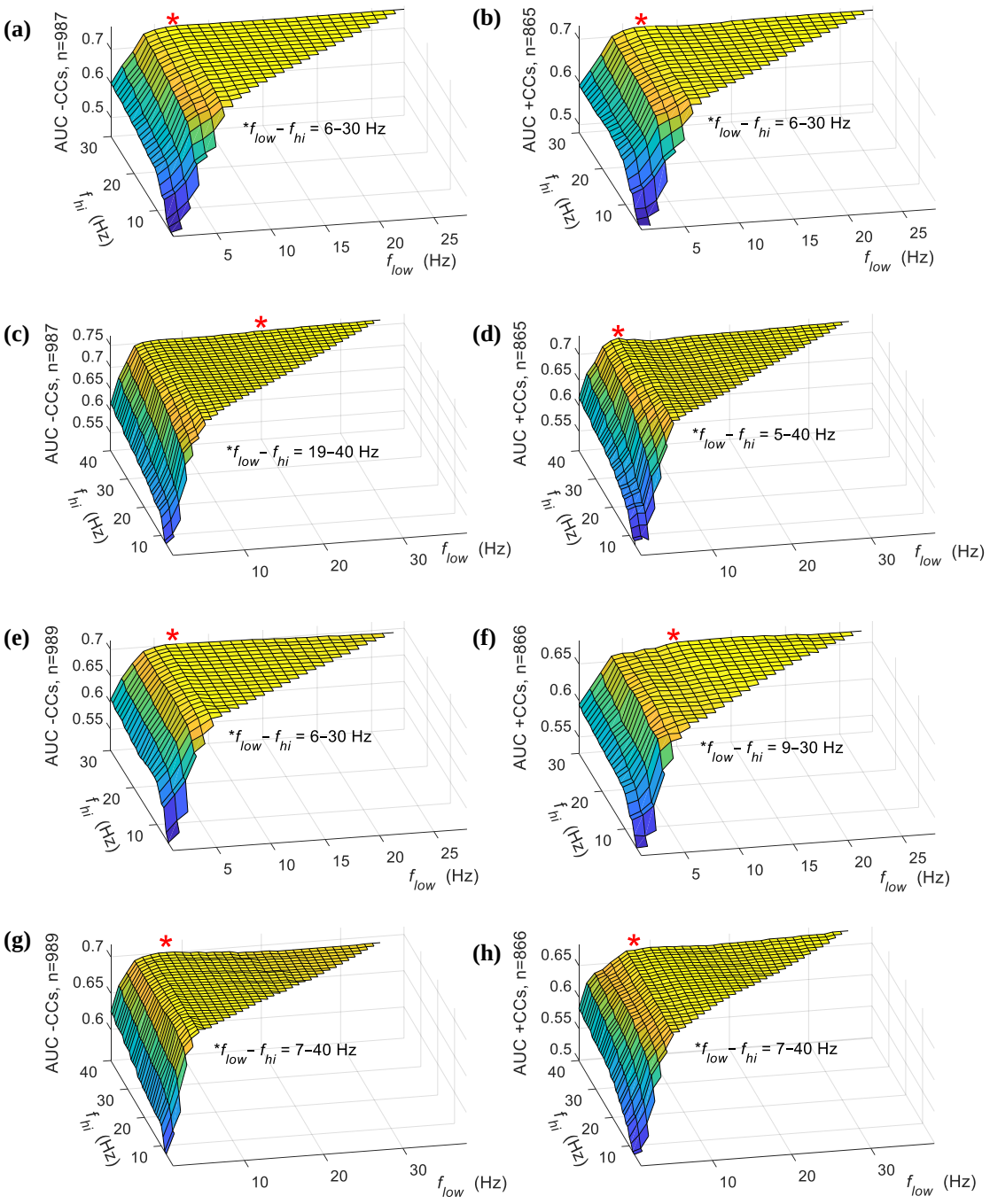

Figure 12. *Shannon Energy* parameter selection
Parameter selections based on training data area under the receiver operating characteristic curve (AUC) for *Shannon Energy* for predicting survival using filtered data (a) without compressions (-CCs) and (b) with compressions (+CCs), for predicting survival using unfiltered data (c) -CCs and (d) +CCs, for predicting return of rhythm using filtered data (e) -CCs and (f) +CCs, and for predicting return of rhythm using unfiltered data (g) -CCs and (h) +CCs.

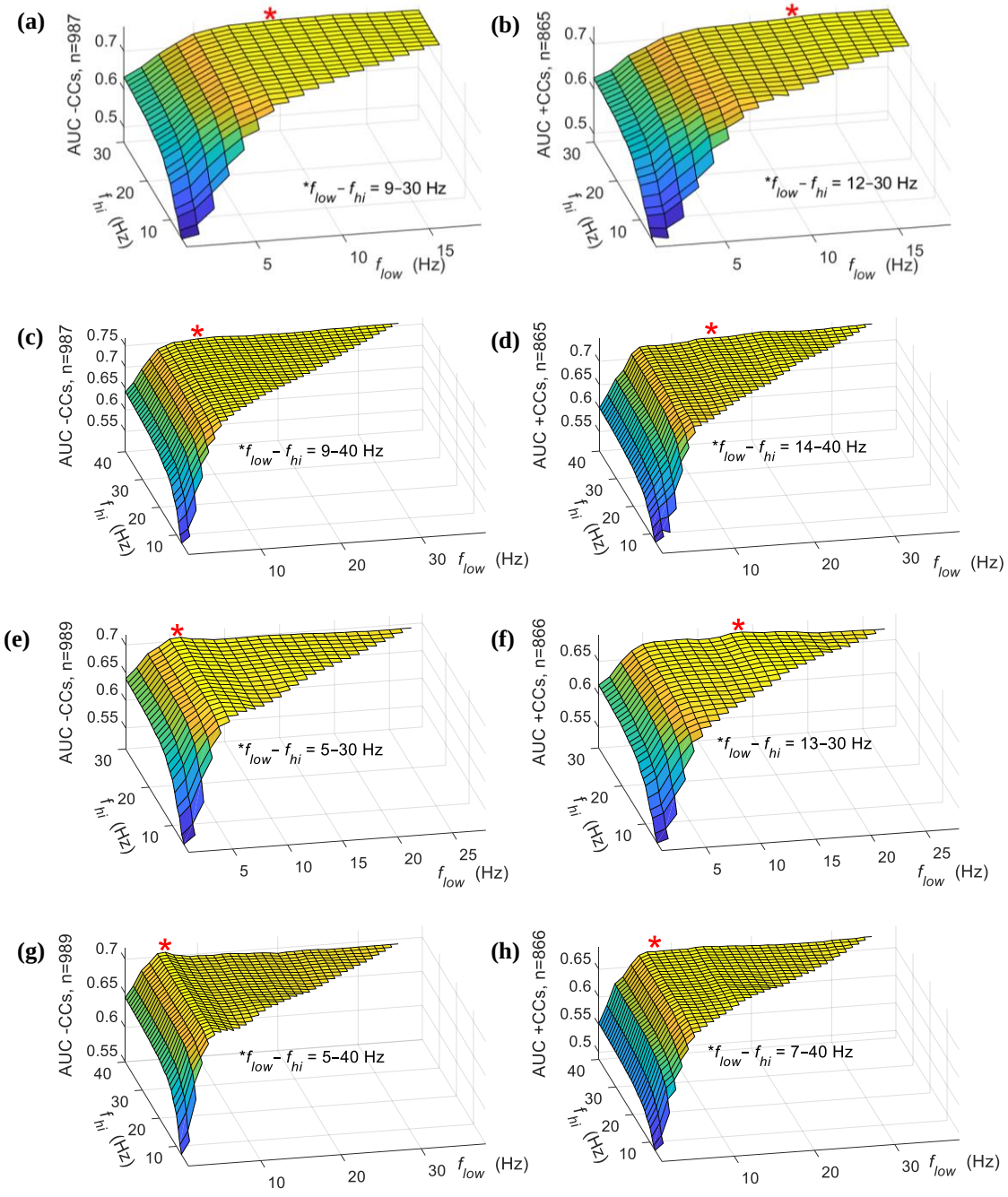

Figure 13. ***Interfrequency Shannon Energy*** **parameter selection**
Parameter selections based on training data area under the receiver operating characteristic curve (AUC) for *Interfrequency Shannon Energy* for predicting survival using filtered data (a) without compressions (-CCs) and (b) with compressions (+CCs), for predicting survival using unfiltered data (c) -CCs and (d) +CCs, for predicting return of rhythm using filtered data (e) -CCs and (f) +CCs, and for predicting return of rhythm using unfiltered data (g) -CCs and (h) +CCs.

D. ECG Dominant Frequency Features with Parameter Selections

Brown et al. first demonstrated an association between the median frequency in the VF Fourier spectrum and VF duration, with VF frequency generally observed to decrease as ischemia persists in the myocardium and the likelihood of successful defibrillation is reduced.[35] Further metrics to describe the dominant frequency in the Fourier spectrum of the VF signal, such as centroid power and peak frequency, also have been proposed by Brown et al. and Eftestol et al.[36,37] However, such methods are limited by the Fourier spectrum and do not account for variations over time. Watson et al. therefore subsequently proposed improved scalogram-based estimators of mean and peak frequency in the VF signal to account for variations in frequency over time.[18]

In the current investigation we characterized the dominant frequency in the VF ECG calculated from the scalogram. In general, VF with good prognosis has a higher dominant frequency than VF with poor prognosis (e.g. Figure 14). To provide an alternative descriptor of dominant frequency in contrast to prior methods such as those proposed by Watson et al., we optimized a specific frequency cutoff indicative of robust VF physiology and calculated the proportion of time the dominant VF frequency exceeded the cutoff. Specifically, we calculated the wavelet *Maxima Fraction* as

$$Maxima\ Fraction = \frac{\sum_{n=0}^{N-1} \sigma_n}{N}, \tag{13}$$

where to determine σ_n at each sample index $0,...n...,N-1$,

$$\sigma_n = \begin{cases} 1 & \text{if } m_n > f_c \\ 0 & \text{if } m_n \le f_c \end{cases}, \tag{14}$$

given

$$m_n = \arg\max_f (|w_n|), \tag{15}$$

where $w_{n,f}$ are the wavelet transform coefficients at sample indices n across frequencies f (in Hz) and f_c is a frequency threshold parameter. Hence, the *Maxima Fraction* can be understood as the proportion of time the dominant VF frequency m_n in the scalogram exceeds f_c (Figure 15). To further describe the overall dominant frequency of the VF signal we also calculated the *Mean Maxima*, the average dominant frequency (in Hz) over the course of the input signal, as

$$Mean\ Maxima = \frac{1}{N}\sum_{n=0}^{N-1} m_n\,, \tag{16}$$

where again,

$$m_n = \arg\max_f \left(\left|w_{n,f}\right|\right), \tag{17}$$

and $w_{n,f}$ are the wavelet transform coefficients at sample indices n and frequencies f (Figure 15).

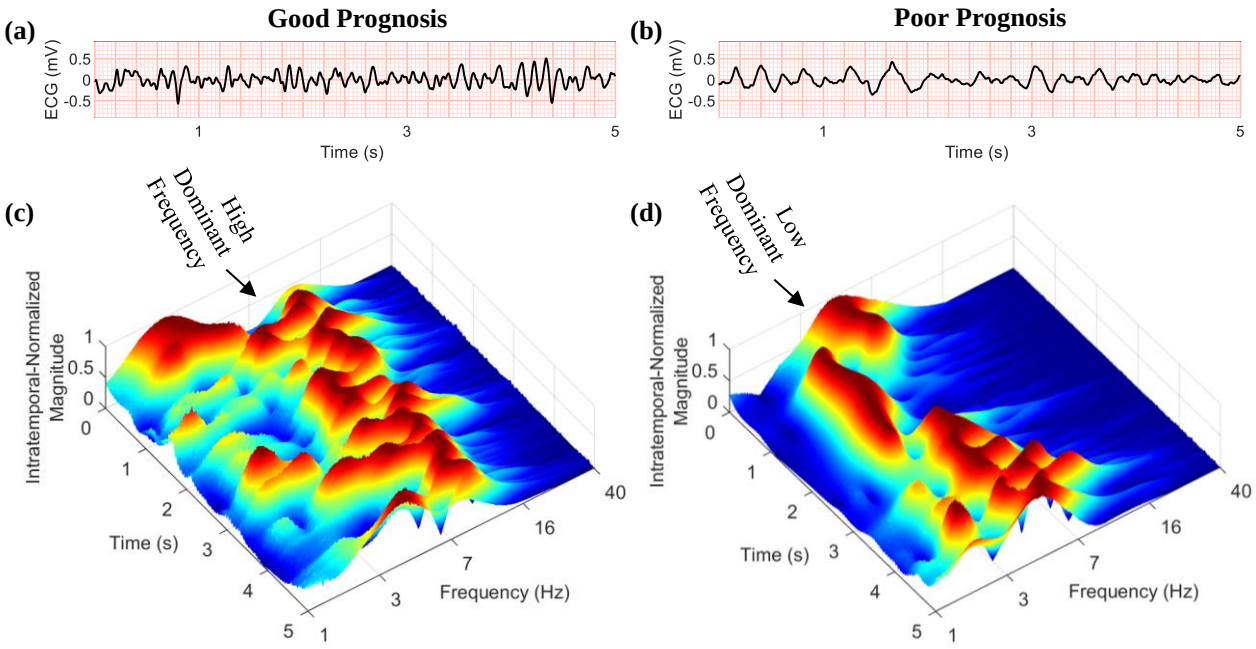

Figure 14. Example of VF with good versus poor prognosis
(a) VF ECG without chest compressions that was subsequently successfully defibrillated (i.e. good prognosis). (b) VF ECG without chest compressions that subsequent shock failed to defibrillate (i.e. poor prognosis). (c) The intratemporal-normalized scalogram of VF with good prognosis indicates overall relatively high dominant frequency (between approximately 6-13 Hz). (d) The intratemporal-normalized VF with poor prognosis indicates overall relatively low dominant frequency (between approximately 2-7 Hz).

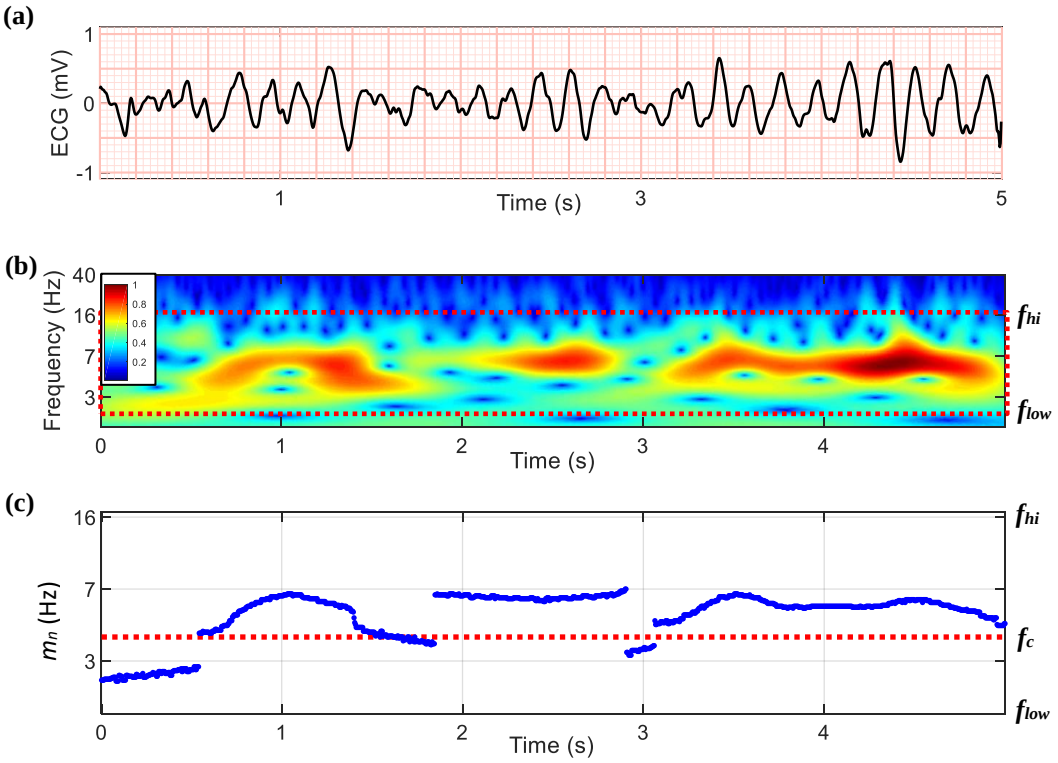

Figure 15. ***Maxima Fraction*** **and** ***Mean Maxima*** **example**
(a) VF ECG without chest compressions. In this example, the VF signal has a good prognosis (i.e. large amplitude and higher dominant frequency) and resulted in return of rhythm after subsequent shock. (b) Scalogram of VF during compressions normalized to a maximum of 1. (c) Maxima m_n at each time sample relative to the variable threshold, f_c ; dominant frequencies above this threshold are indicative of good prognosis. The time-series maxima m_n represent the dominant frequency of the signal.

We varied parameters for *Maxima Fraction* and *Mean Maxima* to optimize performance with and without compressions (Figure 16 and Figure 17). For *Maxima Fraction* optimization, the frequency threshold value f_c indicative of robust VF (see Figure 15) was varied to maximize AUC on training data. This optimization thus attempts to define a specific dominant frequency threshold value indicating good prognosis for an individual VF segment. The frequency range for evaluation of the *Maxima Fraction* was fixed at [f_{low}, f_{hi}] = [2.6 Hz, 41.6 Hz] (corresponding to wavelet scale factors of a=95 and a=6), which is above the typical fundamental frequency of chest compressions (i.e. approximately 1.2-2.5 Hz) but otherwise encompasses wide bandwidth. This enables the function to track the time-series dominant frequency m_n between the widest reasonable range of frequencies, to allow proper comparison of dominant frequency m_n against the threshold frequency f_c.

In contrast, for the *Mean Maxima*, the frequency range [f_{low}, f_{hi}] for evaluation of the function was varied to give the function greater flexibility to ignore potential low-frequency chest compression artifact or high-frequency noise. When optimizing [f_{low}, f_{hi}] for *Mean Maxima*, the widest absolute frequency range corresponding to a training AUC within +/- 0.005 of the maximum AUC was selected to prevent overfitting to local AUC maxima and enabling the widest usable bandwidth.

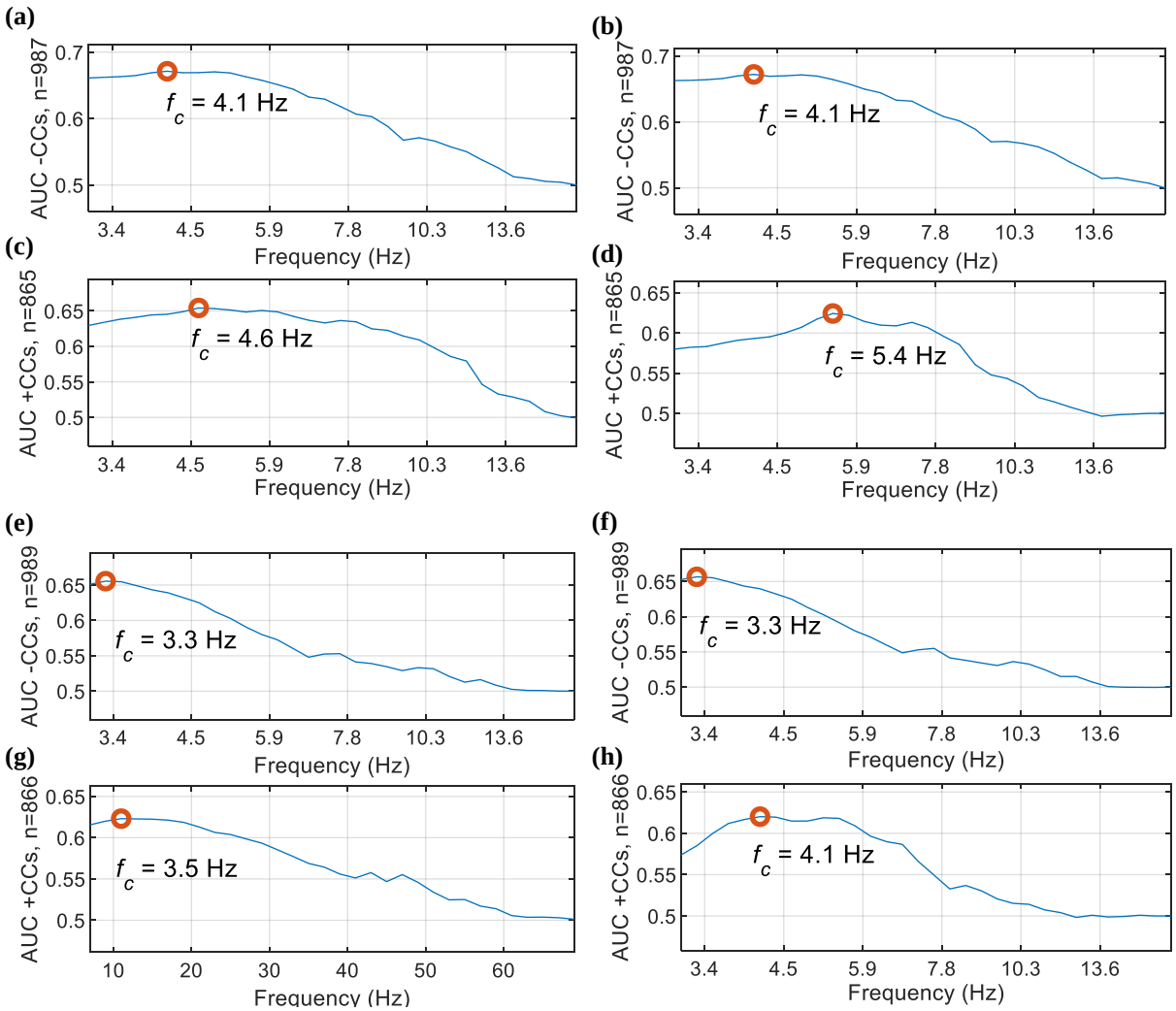

Figure 16. ***Maxima Fraction*** **parameter selection**
Selections of the frequency cutoff f_c indicative of VF with good prognosis are illustrated based on training AUC. Results are shown for (a) predicting survival -CCs using filtered data, (b) predicting survival -CCs using unfiltered data, (c) predicting survival +CCs using filtered data, (d) predicting survival +CCs using unfiltered data, (e) predicting return of rhythm -CCs using filtered data, (f) predicting return of rhythm -CCs using unfiltered data, (g) predicting return of rhythm +CCs using filtered data, and (h) predicting return of rhythm +CCs using unfiltered data. (AUC = area under receiver operating characteristic curve, -CCs = without chest compressions, +CCs = with chest compressions.)

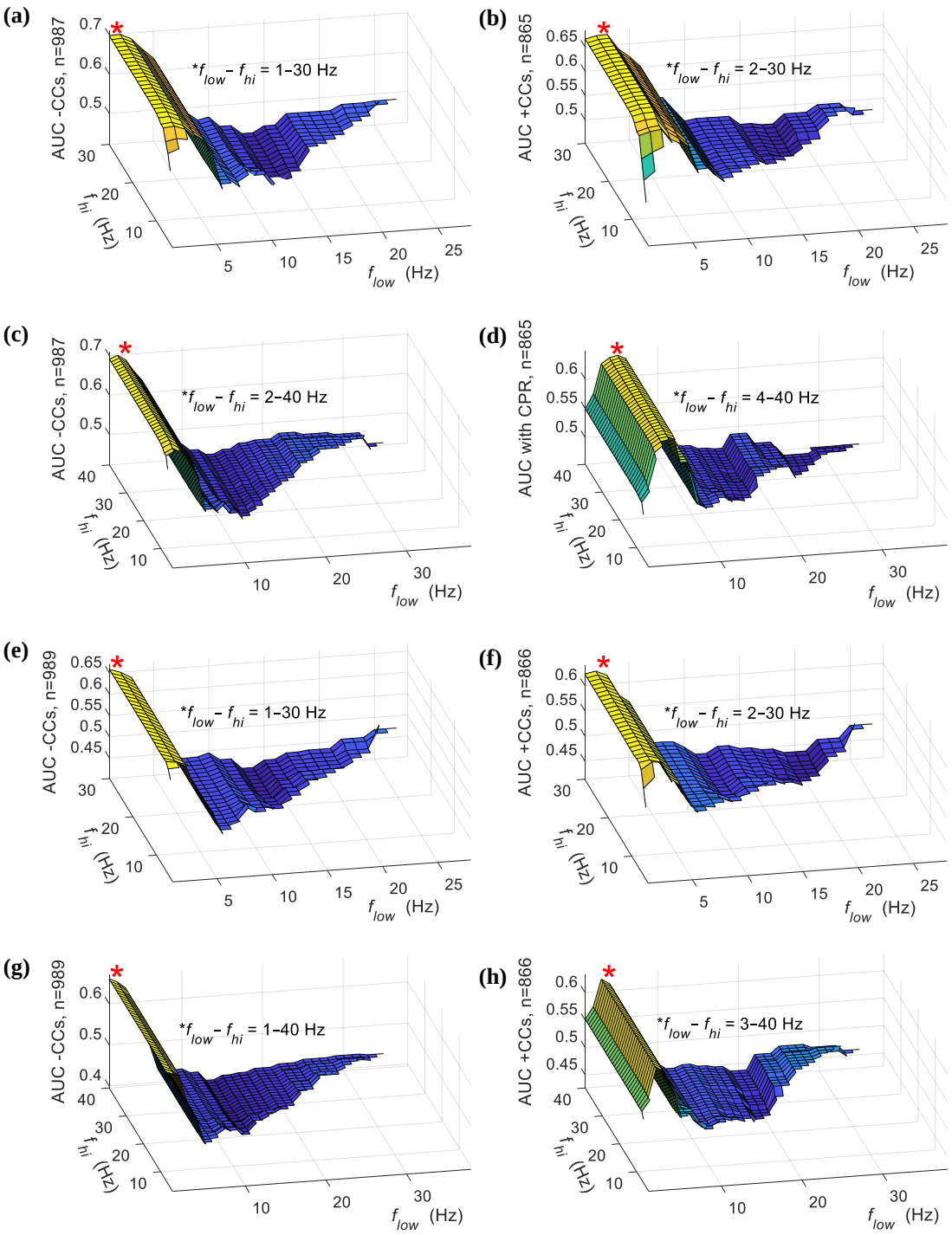

Figure 17. *Mean Maxima* parameter selection

Mean Maxima frequency ranges [f_{low}–f_{hi}] are selected using AUC on training data. Results are shown for predicting survival using filtered data (a) -CCs and (b) +CCs, for predicting survival using unfiltered data (c) -CCs and (d) +CCs, for predicting return of rhythm using filtered data (e) -CCs and (f) +CCs, and for predicting return of rhythm using unfiltered data (g) -CCs and (h) +CCs. (AUC = area under the receiver operating characteristic curve, -CCs = without chest compressions, +CCs = with chest compressions.)

E. ECG Short-Time Fourier Transform Features with Parameter Selections

The short-time Fourier transform can be computed by evaluating the discrete Fourier transform of windowed segments of the input signal to provide a time-varying representation of the signal's spectrum. The general discrete form is $X(m,\omega)=\sum_{n} x_n w_{n-m} e^{-j\omega n}$, given slow-time index m (where *m* is the index of the current window), time-domain input x_n of length N and sampling index n, window w, and discretized frequency ω. The Morlet wavelet transforms employed in the previous sections provide excellent temporal and frequency separation, and are therefore considered superior to short-time Fourier transforms for the purpose of ECG analysis and feature extraction.[17,18] Therefore, to complement the wavelet-based features which employed a fine, fixed temporal resolution, we calculated coarse short-time Fourier transforms with variable window sizes to provide an alternative representation of the VF signal with spectral content averaged over longer time segments as compared to the Morlet wavelet time-frequency transforms. Specifically, we derived two features of the VF ECG (the *Short-Time Deviation* and the *Correlation Component*) using relatively coarse short-time Fourier transforms. The transforms were calculated using a sliding box window with no window overlap.

Specifically, to describe the overall standard deviation of the spectrum magnitudes at each time index, the *Short-Time Deviation* was calculated as

$$\textit{Short-Time Deviation} = \text{median}(s_{0,\ldots m\ldots,M-1}), \tag{18}$$

where

$$s_m = \sqrt{\frac{1}{(j_{hi}-j_{low})}\sum_{j=j_{low}}^{j_{hi}} (X_{m,j}-\bar{X}_m)^2}, \tag{19}$$

$X_{m,j}$ are the root-magnitude values of the discrete Fourier transform at window index m normalized to a maximum of 1, the frequency indices j for $j_{low} \le j \le j_{hi}$ correspond to the range of frequencies $[f_{low}, f_{hi}]$ (in Hz) selected for analysis, $\bar{X}_m$ designates the mean of X_m at a single window index m between frequency indices $j_{low} \le j \le j_{hi}$, and M is the short-time window length in samples (Figure 18).

To describe the change in the VF spectrum and to quantify the similarities of the magnitude profiles over time between different frequencies, we calculated the *Correlation Component* from the correlation between time profiles at each frequency index in the short-time Fourier transform. As described above, $X_{m,j}$ represents the root-magnitude at time window index m and frequency index j. We calculated the correlation matrix R of size JxJ comparing the short-time Fourier transform root-magnitude profiles across all time indices m between all possible pairs of frequencies j, where the frequency indices j are between frequency index limits $j_{low} \le j \le j_{hi}$ corresponding to frequency limits $[f_{low}, f_{hi}]$, the number of frequency bins analyzed $J = j_{hi} - j_{low} + 1$, and R represents the matrix of correlations between the vectors X_j of spectral magnitudes over time at each frequency index j. Thus,

$$R = \begin{pmatrix} r(X_{j_{low}}, X_{j_{low}}) & \cdots & r(X_{j_{low}}, X_{j_{hi}}) \\ \vdots & \ddots & \vdots \\ r(X_{j_{hi}}, X_{j_{low}}) & \cdots & r(X_{j_{hi}}, X_{j_{hi}}) \end{pmatrix}, \tag{20}$$

where $r(X_{j_1}, X_{j_2})$ represents the Pearson correlation between the time-series root magnitude profiles at frequency indices j_1 and j_2 (Figure 18). Then, to represent the amount of variance for the orthogonal characteristics of R for the current ECG segment, the *Correlation Component* is represented using principal component analysis of the matrix *R* as

$$Correlation\ Component = p_c\,, \tag{21}$$

where p_c is equal to the variance score of the c^{th} principal component (i.e., c^{th} sorted eigenvalue) of principal component analysis of the matrix R (Figure 18c).

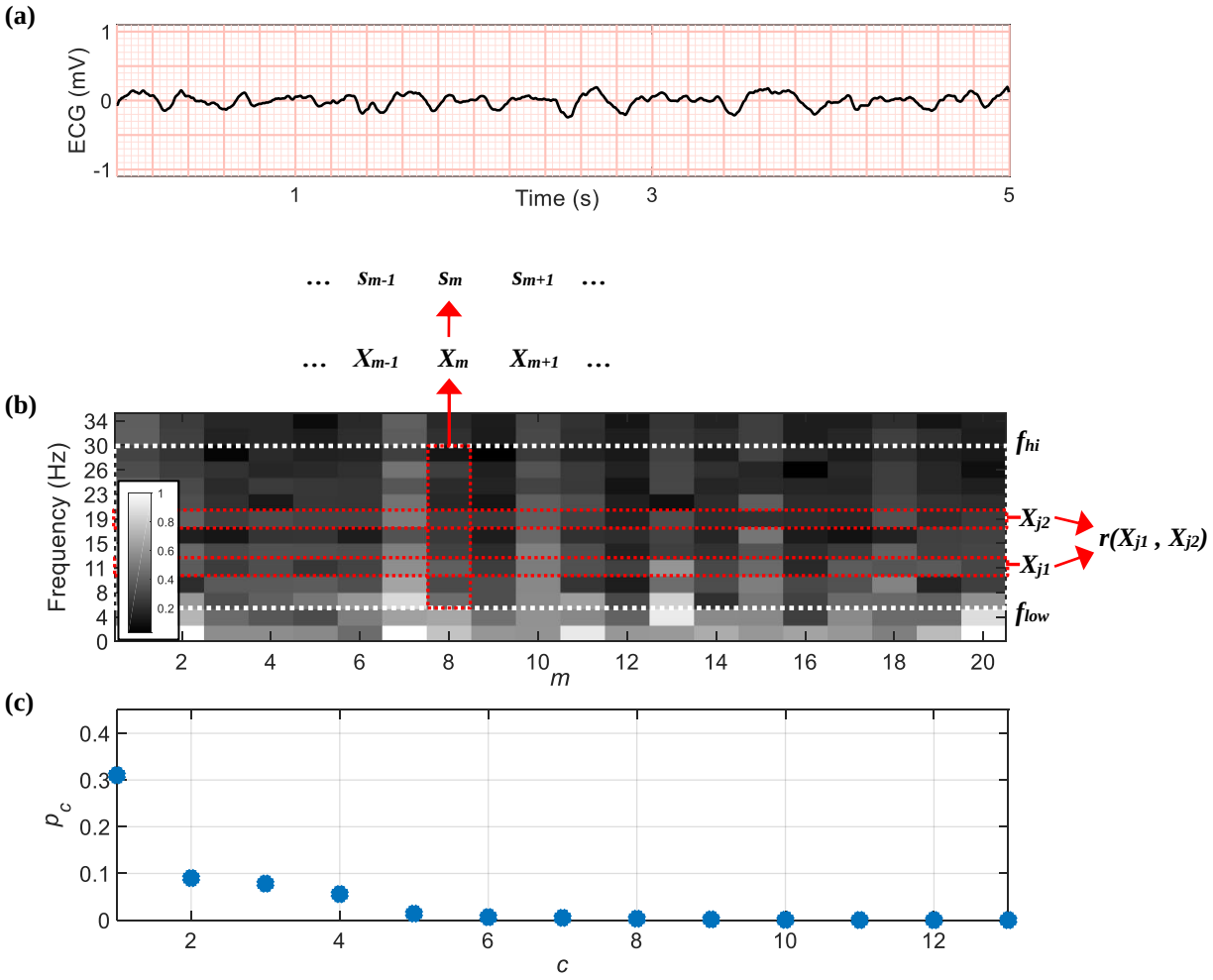

Figure 18. *Short-Time Deviation* and *Correlation Component* example
(a) VF without chest compressions. In this example (in contrast to Figure 15a), the VF signal has a poor prognosis (i.e. lower amplitude and frequency) and did not result in return of rhythm after subsequent shock. (b) Low-resolution short-time Fourier transform of VF without compressions. (c) Sorted principal component variances p_c (i.e. eigenvalues) of principal component analysis of the Pearson correlation matrix R calculated from magnitudes X_m for the current ECG segment.

We selected parameters to optimize the prognostic performance of the *Short-Time Deviation* and *Correlation Component* features. Specifically, the time and frequency resolutions

of the time-frequency transform were varied to maximize AUC on training data. For both functions, the time resolution as governed by the sliding window size M (in samples) was varied, with results shown in Figure 19, Figure 20. The frequency resolution Δf (in Hz) at each window index *m* for evaluation of *Short-Time Deviation* was increased proportionally to time resolution and can be calculated as $\Delta f = \frac{f_s}{5(N/M)}$, given sampling rate f_s and ECG input length N. In contrast, the frequency resolution for evaluation of *Correlation Component* was fixed at $\Delta f = 2.5$ Hz. To avoid low-frequency chest compression artifact, frequency limits (in Hz) for evaluation of *Short-Time Deviation* were calculated as $[f_{low}, f_{hi}] = [2(\Delta f), f_s/6]$. Likewise, frequency limits (in Hz) for calculation of *Correlation Component* were fixed at $[f_{low}, f_{hi}] = [5, f_s/6]$. The *Correlation Component* index parameter c was selected as $c = 2$; i.e., the score value of the second-largest eigenvalue was used as the output of the *Correlation Component*.

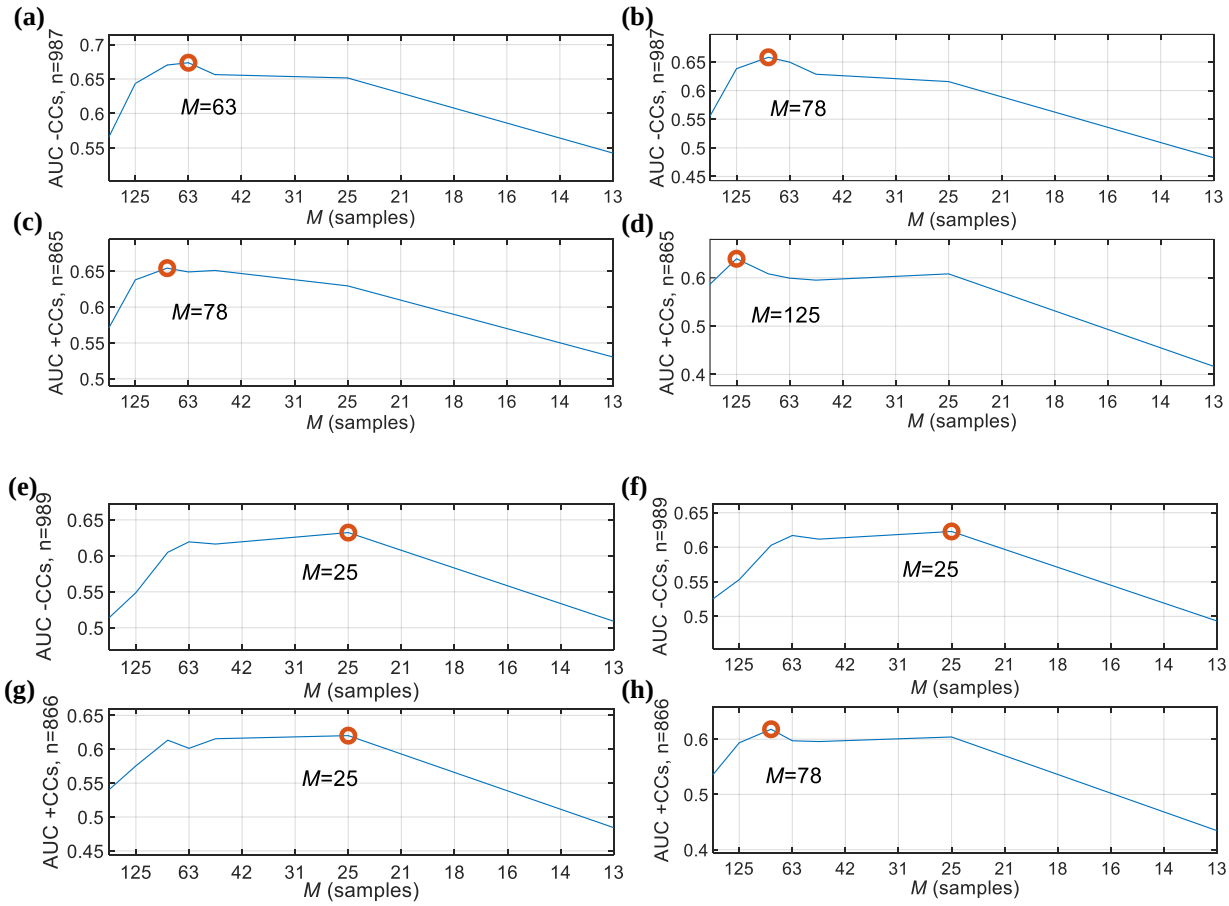

Figure 19. *Short-Time Deviation* parameter selection
Selections of window size *M* are illustrated based on training AUC. Results are shown for (a) predicting survival -CCs using filtered data, (b) predicting survival -CCs using unfiltered data, (c) predicting survival +CCs using filtered data, (d) predicting survival +CCs using unfiltered data, (e) predicting return of rhythm -CCs using filtered data, (f) predicting return of rhythm -CCs using unfiltered data, (g) predicting return of rhythm +CCs using filtered data, and (h) predicting return of rhythm +CCs using unfiltered data. (AUC = area under receiver operating characteristic curve, -CCs = without chest compressions, +CCs = with chest compressions.)

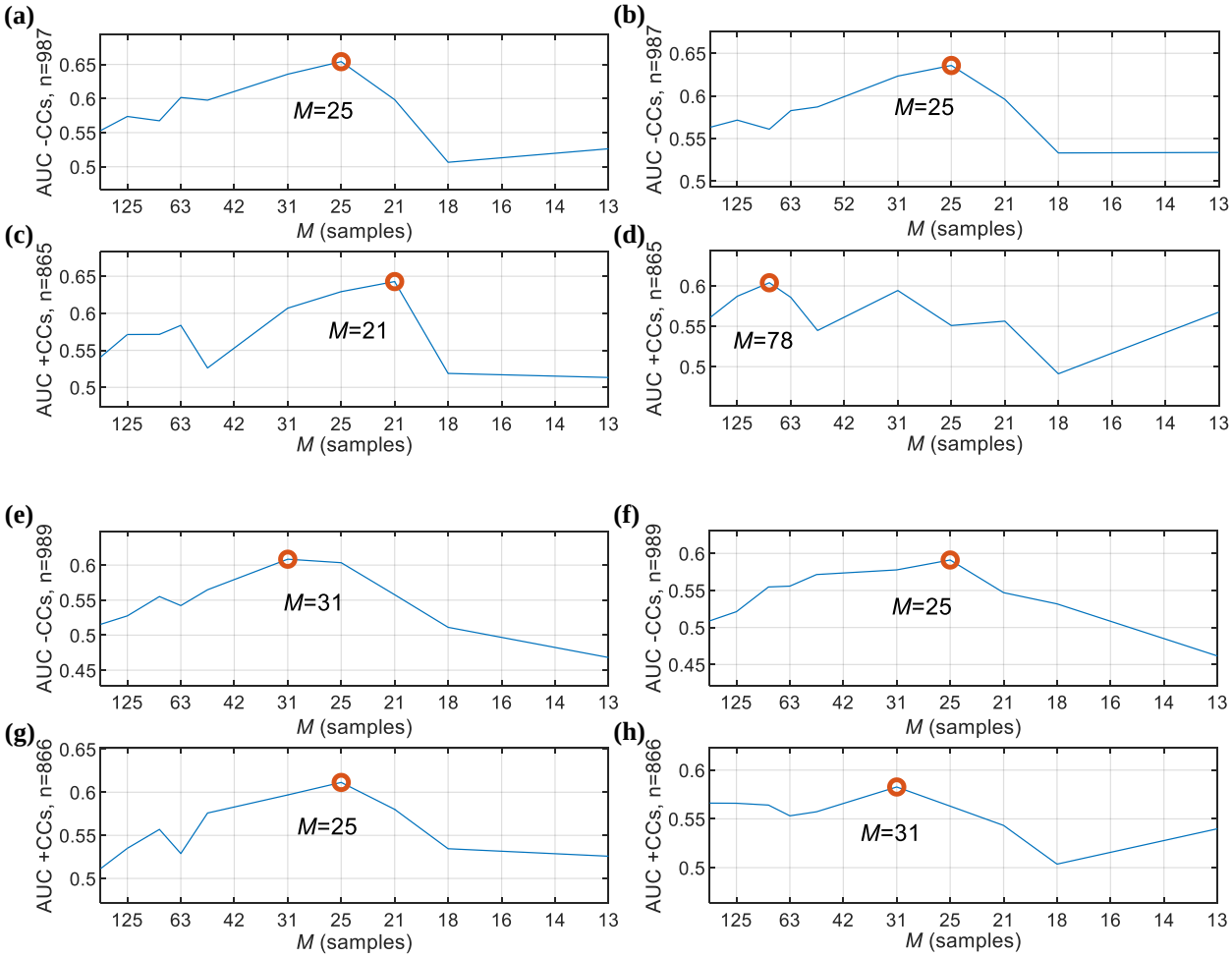

Figure 20. *Correlation Component* parameter selection
Selections of window size *M* are illustrated based on training AUC. Results are shown for (a) predicting survival -CCs using filtered data, (b) predicting survival -CCs using unfiltered data, (c) predicting survival +CCs using filtered data, (d) predicting survival +CCs using unfiltered data, (e) predicting return of rhythm -CCs using filtered data, (f) predicting return of rhythm -CCs using unfiltered data, (g) predicting return of rhythm +CCs using filtered data, and (h) predicting return of rhythm +CCs using unfiltered data. (AUC = area under receiver operating characteristic curve, -CCs = without chest compressions, +CCs = with chest compressions.)

F. Support Vector Machine Training and Parameter Selections

Support vector machines are binary classifiers that discriminate data using the principle of a maximally-separating hyperplane defining the boundaries between classes. The class of an unknown $N-$dimensional input x_{input} is predicted based on its position relative to the separating hyperplane, where N is the number of input features. The hyperplane itself is defined by T $N-$dimensional training points (support vectors) , x_t, which support the classification boundaries in the $N-$dimensional feature space. Furthermore, the support vectors can be mapped to a higher-dimensional feature space using a kernel function K to allow construction of a hyperplane in this higher-dimensional space that may allow improved separation than a discriminant in the $N-$dimensional feature space.[38,39] In effect, such a classifier may be considered as evaluating the sum of similarities between unknown inputs x_{input} and known support vector training points x_t (and the associated training class assignments $y_t \in \{-1,1\}$). The sign of the summation of similarities determines the position of the unknown point versus the decision boundary and indicates the class prediction. Specifically, the output of a support vector machine employing a kernel function is of the form

$$f(x) = \sum_{t=1}^{T} y_t \alpha_t K(x_{input}, x_t) + w_0, \tag{22}$$

where α_t are model parameters and w_0 is a constant. Typically the predicted class is interpreted as $\text{sgn}(f(x))$. While a variety of kernel functions K are available to evaluate similarity between a known sample and unknown sample, we selected the radial (Gaussian) kernel which in effect allows nonlinear boundaries and enables model regularization through adjustment of the kernel size parameter. Using the radial kernel, the similarity between $N-$dimensional arbitrary samples

a and b is evaluated by $K(a,b) = \exp(-\gamma \sum_{j=1}^{N} \left(a_j - b_j\right)^2)$, where γ is a positive constant that controls the size of the gaussian curve used to evaluate similarity (thus affecting the smoothness of the decision boundary). The objective function minimized during training is of the form $\frac{1}{2}\|w\|^2 + C\left(\sum_{t=1}^{T} \xi_t\right)$, where w represents parameter weights, the slack variable ξ represents the degree of misclassification for each training point, and the slack penalty C (also referred to as box constraint) is a constant that controls the relative weight of the misclassification error during minimization. To perform model regularization and control the bias-variance tradeoff during training, both the kernel size γ and box constraint C hyperparameter constants may be adjusted. Of note, prior VF prognosis studies with support vector machines have held a fixed $C = 1$ and variable γ, which may have limited performance in these prior studies.[40,41]

In the current investigation, we trained support vector machine models to predict patient outcome using ten novel features of the VF ECG. Inputs were transformed using natural logarithm to improve normality of their distributions. Rather than threshold outputs as $\text{sgn}(f(x))$, support vector machine output scores for each sample were converted to estimated posterior probabilities via the MATLAB function fitSVMPosterior(), which uses regularized binomial maximum likelihood estimation and cross-validation to train a two-parameter sigmoid mapping function to convert raw model output scores to estimated continuous probability values.[42] The general function to map the support vector machine score $f(x)$ (from Eq. 22 above) to a posterior probability representing likelihood of positive outcome $P(y=1)$ can be represented by $P(y=1 \mid f(x)) = \left[1 + e^{Af(x)+B}\right]^{-1}$ where A, B are parameters of the sigmoid function. The parameters are trained using 10-fold cross-validation on the study training data. To improve the

normality of posterior probability output scores, we applied a logit transformation to the scores (Figure 21). Four support vector machine models were trained (for use with compressions and without compressions to predict survival and return of rhythm).

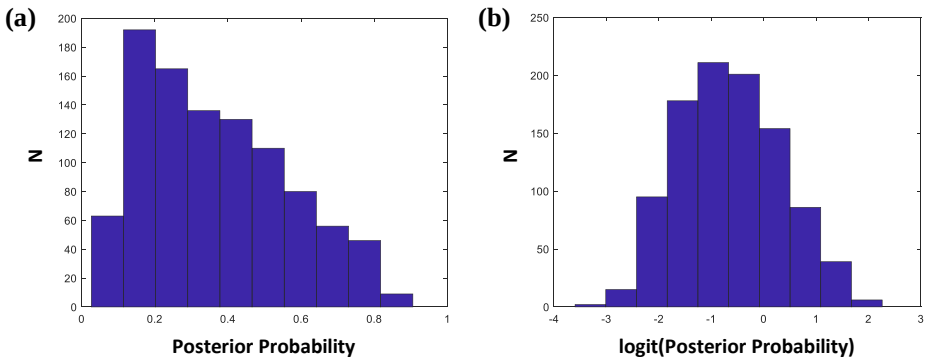

Figure 21. Support vector machine score distribution example
Support vector machine examples output distribution for prediction of survival during CPR on training data. The posterior probability values produced by the sigmoid mapping function applied to raw support vector machine scores calculated from training data, shown in (a), are skewed left. The logit transform was thus applied to these posterior probability scores to improve the normality of the distribution, as shown in (b).

We optimized both kernel size γ and box constraint C hyperparameters using training data by performing a grid search of 5-fold cross-validation error values versus hyperparameter values (Figure 22). To improve generalizability, we underfit the model. A tolerance error value τ was applied during support vector machine training such that during the grid search of error versus hyperparameter values, the maximum γ and minimum C was determined subject to the constraint $\tau \geq \left| error_{\gamma,C} - \min(error) \right|$, where $error_{\gamma,C}$ represents the cross-validation error at a particular (γ, C) combination, and $\min(error)$ represents the minimum observed error over all hyperparameter combinations.[23] This procedure slightly increased the selected kernel size and slightly decreased the selected box constraint while still maintaining an overall cross-validation error within a small tolerance of the global minimum observed error in the search grid. Different tolerances were

selected for each hyperparameter. The minimum C was selected such that $\tau_C \geq \left| error_{\gamma,C} - \min(error) \right|$, and then the maximum γ was selected with C fixed such that $\tau_\gamma \geq \left| error_{\gamma,C} - \min(error) \right|$. We used τ_C = 0.035 for data without compressions, τ_C = 0.035/2 for data with compressions (as compression-artifacted data had more class overlap), and τ_γ = 0.003.

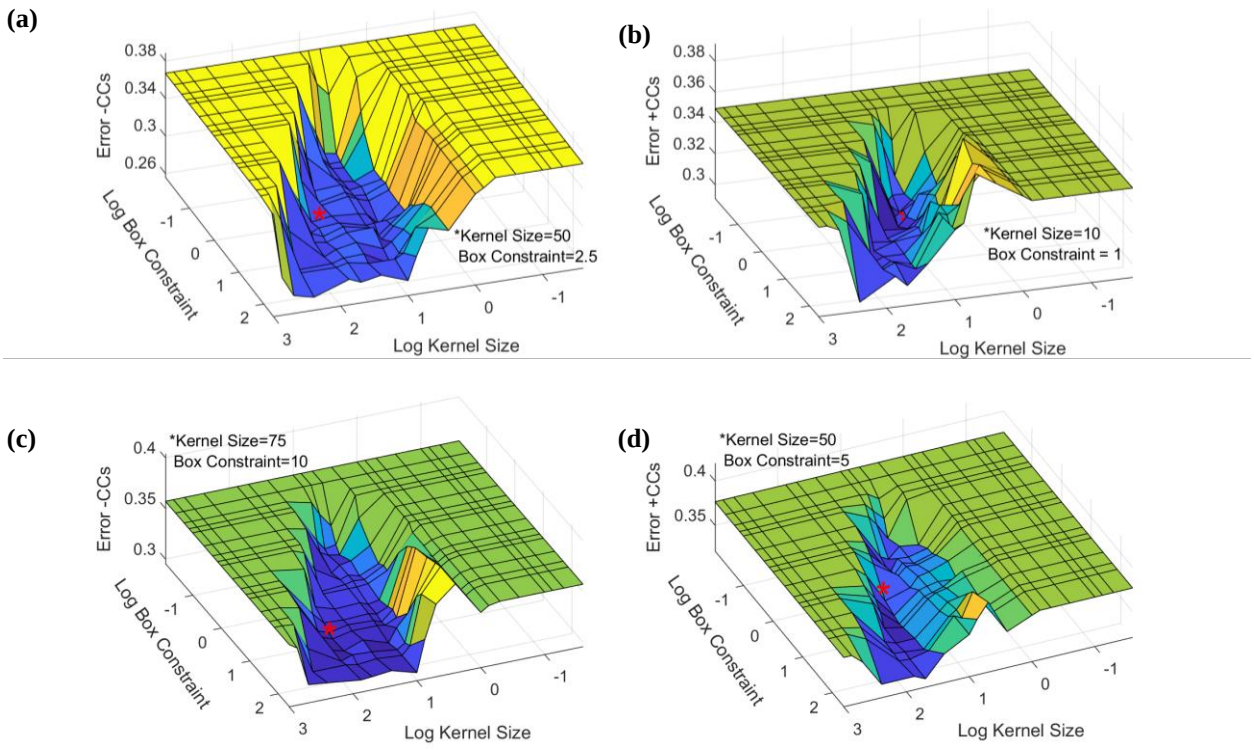

Figure 22. Support vector machine hyperparameter selection
Box constraint and kernel size values (C and γ) selected to minimize 5-fold cross validation error on training data. Values (*) are selected as the minimum box constraint and maximum kernel sizes within the error tolerance τ from the absolute minimum error. Results are shown to (a) predict survival -CCs, (b) predict survival +CCs, (c) predict return of rhythm -CCs, and (d) predict return of rhythm +CCs. (-CCs = without chest compressions, +CCs = with chest compressions.)

G. Validation Performance of Individual ECG Features

The current method calculated ten ECG features in parallel from both unfiltered ECGs and filtered ECGs. On validation data, ECG features evaluated individually predicted study outcomes with AUC values ranging from 0.52-0.75 (Table 2, Table 3).

Table 2. Validation AUC values for individual features (predicting defibrillation success)
Validation AUC values for prediction of return of organized rhythm after shock using individual ECG features calculated with filtered and unfiltered VF segments from 691 validation patients are reported. For comparison, validation AUC values for the support vector machine (SVM) combination of all 20 (10 filtered and 10 unfiltered) features and for the final logistic model (incorporating patient characteristics) are also reported.

Feature	**Without Chest Compressions**		**With Chest Compressions**	
	ECG Filter: 1-30 Hz	ECG Filter: Unfiltered	ECG Filter: 1-30 Hz + Notch	ECG Filter: Unfiltered
Sliding Deviation	0.746	0.745	0.687	0.653
Sliding Peak	0.725	0.723	0.667	0.581
Interfrequency Entropy	0.606	0.606	0.538	0.632
High-Frequency Entropy	0.567	0.611	0.493	0.526
Shannon Energy	0.731	0.725	0.670	0.669
Interfrequency Shannon Energy	0.736	0.739	0.678	0.688
Wavelet Maxima	0.683	0.681	0.636	0.639
Wavelet Maxima Fraction	0.675	0.677	0.648	0.650
Short-Time Deviation	0.668	0.659	0.615	0.644
Correlation Component	0.641	0.588	0.598	0.573
SVM Combination of Filtered and Unfiltered ECG Features	0.748		0.695	
Full Logistic Model incorporating SVM + Dichotomous Variables	0.769		0.740	

Table 3. Validation AUC values for individual features (predicting functional survival)
AUC values for prediction of functional survival using individual ECG features calculated with filtered and unfiltered VF segments from 691 validation patients are reported. Validation AUC values for the support vector machine (SVM) combination of all 20 (10 filtered and 10 unfiltered) features and for the final logistic model (incorporating patient characteristics) are also reported.

Feature	Without Chest Compressions		With Chest Compressions	
	ECG Filter: 1-30 Hz	ECG Filter: Unfiltered	ECG Filter: 1-30 Hz + Notch	ECG Filter: Unfiltered
Sliding Deviation	0.729	0.735	0.728	0.694
Sliding Peak	0.672	0.689	0.690	0.614
Interfrequency Entropy	0.678	0.677	0.624	0.676
High-Frequency Entropy	0.574	0.599	0.589	0.561
Shannon Energy	0.753	0.747	0.735	0.741
Interfrequency Shannon Energy	0.752	0.754	0.732	0.740
Wavelet Maxima	0.710	0.715	0.685	0.684
Wavelet Maxima Fraction	0.702	0.701	0.683	0.664
Short-Time Deviation	0.707	0.673	0.666	0.660
Correlation Component	0.631	0.602	0.637	0.584
SVM Combination of Filtered and Unfiltered ECG Features	0.751		0.746	
Full Logistic Model incorporating SVM + Dichotomous Variables	0.762		0.753	

Of the ten ECG features, two were developed based on ECG amplitude: *Sliding Deviation* and *Sliding Peak*. Both amplitude features had relatively high performance without compressions but were significantly affected by compression artifact. The optimal analysis window size was as short as 16 ms during compressions. While the optimal length even without compressions was longer than the length during compressions, it did not exceed 72 ms. Within a window size of 72 ms, full-period oscillations at approximately ≥14 Hz may be observed, and since both amplitude functions operate on the absolute-value, zero-mean ECG (i.e. negative fluctuations below baseline are translated to positive fluctuations, thus doubling the occurrence of positive peaks), a full period of rotors resulting from a native ≥7 Hz source may theoretically be observed within such a window size. These observations suggest that high-frequency amplitude in VF is predictive of patient outcome and that lower-frequency amplitude fluctuations (i.e. below approximately 7 Hz) in the waveform, while useful, may be ignored to reduce the effect of chest compression artifact in amplitude-based analysis.

Four features were designed based on forms of the Shannon equation applied to the scalogram: *Interfrequency Entropy*, *High-Frequency Entropy*, *Shannon Energy*, and *Interfrequency Shannon Energy*. These features incorporate the median operation to exclude spurious behavior within isolated frequency bands and at isolated time points. *Interfrequency Entropy* and *High-Frequency Entropy* features were calculated from probability distributions of scalogram magnitudes across frequencies independent of the absolute energy in each frequency. The wider-band *Interfrequency Entropy* functioned optimally with a high-pass (i.e. lower frequency limit) cutoff of approximately 3-4 Hz both with and without CPR. This result suggests that having evenly-distributed magnitudes across a wide range of frequencies indicates a good prognosis as compared to smoother VF containing only low-frequency content. Prior studies of various entropy metrics of the VF signal have confirmed similar observations of higher entropy values indicating better prognosis.[30,31] However, in contrast, we also observed that when frequency ranges were optimized based on inverse entropy across spectral distributions, the optimal frequency ranges were approximately 15-40 Hz. This result suggests that when limited to high frequencies alone, presence of dominant spectral content in narrow high-frequency bands, rather than an even distribution of spectral content, is also indicative of good prognosis. *Shannon Energy* and *Interfrequency Shannon Energy* were calculated using the Shannon equation applied directly to the non-normalized wavelet transform coefficient magnitudes. Increased energy was associated with positive outcome, and analyses limited to higher frequencies performed best. The two Shannon energy features had the most robust performance during compressions of any individual metrics, suggesting that increased high-frequency energy (between approximately 10-40 Hz) is a superior indicator of good prognosis versus other metrics, especially during CPR. This result

confirms similar observations of time-frequency energy metrics in our benchmark of existing ECG features during CPR.[23]

Two features were applied to describe the dominant frequency of the VF waveform: *Maxima Fraction* and *Mean Maxima*. Rather than estimating dominant, peak, or centroid VF frequency from the Fourier transform as in prior studies, *Maxima Fraction* and *Mean Maxima* track dominant VF frequency over time using the scalogram.[22,35,37,43,44] *Maxima Fraction* evaluated the proportion of time the VF frequency exceeds a threshold indicative of good prognosis. While the exact VF dynamics in humans are uncertain, one theory hypothesizes that VF is largely driven by a dominant self-sustaining mother rotor of depolarizing ventricular cardiomyocytes; in contrast, other studies theorize the presence of multiple smaller self-perpetuating rotors.[7,9,45] Therefore it is unclear whether the *Maxima Fraction* is an estimate of a single 'mother' rotor versus an aggregate of multiple contributing rotors. Regardless, our results indicate that a dominant frequency above a threshold at approximately 3.3-5.4 Hz is indicative of good prognosis, while a dominant frequency below this range is associated with poor prognosis, potentially due to prolonged ischemia and reduced conduction velocity. The *Mean Maxima* did not derive a specific threshold defining robust VF but instead applied frequency ranges to allow exclusion of CPR artifact when evaluating dominant frequency. Notably, in contrast to energy and entropy features which still functioned with relatively high performance using only high frequencies (i.e. ≥10 Hz), *Mean Maxima* required mid-frequency content (between 4-10 Hz) for accurate analysis, and had poor performance when limited to high-frequency content only. This result is likely due to the fact that since most human VF is between 3-8 Hz, evaluation of dominant frequency is only useful when describing the fundamental rotor frequency but not for evaluating the sharpness and high frequency harmonic content in the signal above approximately 10 Hz.

Two features were designed to evaluate similarities between the spectra within short-time Fourier transforms of the VF signal: *Short-Time Deviation* and *Correlation Component*. *Short-Time Deviation* evaluated the median flatness of the Fourier magnitudes over short windows of the input signal as described by their standard deviations. A higher median standard deviation of spectral magnitudes was indicative of good prognosis, suggesting that the presence of relatively prominent or fewer rotors in the ventricular myocardium increases the likelihood of successful defibrillation, and more chaotic electrical activity lacking prominent spectral peaks may indicate prolonged VF. These results confirm prior observations that the lack of spectral flatness is a useful predictor of myocardial receptiveness to defibrillation.[36,46] *Correlation Component* evaluated similarities across time profiles between different frequencies. However, utility of this feature was relatively low.

To reduce the effect of chest compression artifact in the ECG and enable continuous analysis throughout resuscitation, the novel algorithm applies a variable-frequency multi-notch filter based on estimated compression frequency if CPR was detected. Because the spectral content of VF is primarily between approximately 3-8 Hz but compression artifacts can affect a range of frequencies that overlap VF frequencies (e.g. 0-20 Hz), the filter reduced narrow fundamental and harmonic CPR frequencies in an attempt to minimize negative effects on the underlying VF signal. We observed that during chest compressions, compression artifact could indeed be attenuated by the variable-frequency filter while still preserving much of the VF ECG signal, improving amplitude-based features during CPR. However, time-frequency features were generally not improved using filtered ECGs versus unfiltered ECGs. In part, this may be due to the inherent ability of time-frequency-based features to exclude compressions after the low frequency limit is optimized. Additionally, filtered ECGs had an upper bandwidth limit of 30 Hz, while unfiltered

ECGs had signal content up to 40 Hz. Based on the optimization results of individual time-frequency features on training data, high-frequency content from 30-40 Hz is useful for predicting outcomes (e.g. Figure 12).

In summary, we calculated ten features of the filtered and unfiltered ECG to predict patient outcomes. During chest compressions, features to quantify high-frequency energy (e.g. 10-40 Hz) had the highest relative performance, while features to describe mid-frequency content (e.g. 4-10 Hz) or amplitude characteristics were increasingly confounded by chest compression artifact. These results are consistent with prior study of VF features during CPR which suggest an advantage using high-frequency energy characteristics.[23,47] Of the individual ECG features, some functioned optimally using filtered data (such as amplitude features sensitive to compression artifact) while others (such as time-frequency features) functioned optimally using unfiltered data due to their ability to leverage additional high-frequency information and inherently exclude frequency-dependent noise.

H. Performance When Missing Age, Sex, and Rhythm History

To evaluate algorithm performance when patient demographics or rhythm history are unavailable, we also trained and evaluated reduced versions of the algorithm that exclude these inputs. Specifically, we first evaluated a reduced version of the algorithm that does not require patient age or sex. We also evaluated a further-reduced model that additionally does not require the ECG rhythm history. The full, reduced, and further-reduced logistic models are represented by:

$$P_{full} = \begin{cases} g\left(\beta_0 + \beta_1(SVM) + \beta_2(Age) + \beta_3(Sex) + \beta_4(Age \times Sex)\right) & \text{if } shock = 1 \\ g\left(\beta_0 + \beta_1(SVM) + \beta_2(Age) + \beta_3(Sex) + \beta_4(Age \times Sex) + \beta_5(Prior\ ROR)\right) & \text{otherwise} \end{cases},$$

$$P_{reduced} = \begin{cases} g\left(\beta_0 + \beta_1(SVM)\right) & \text{if } shock = 1 \\ g\left(\beta_0 + \beta_1(SVM) + \beta_2(Prior\ ROR)\right) & \text{otherwise} \end{cases},$$

$$P_{further-reduced} = g\left(\beta_0 + \beta_1(SVM)\right),$$

where, P represents the probability of successful outcome, the logistic function $g(z) = \frac{1}{1+e^{-z}}$, *shock* represents the current shock cycle number, SVM is the posterior probability output from the support vector machine combination of 10 filtered and 10 unfiltered ECG features, Age, Sex, and $Prior\ ROR$ are dichotomous patient characteristic variables, and β_{0-5} are logistic model parameters.

Validation performance for these reduced models is reported in Table 4. These results suggest that reduced models may still be applied to estimate patient prognosis, and that while inclusion of prior return of organized rhythm has a significant effect on overall model AUC, inclusion of age and sex only provide a marginal benefit to model performance.

Table 4. Algorithm performance for reduced models

AUC (95% confidence interval) for prediction of patient outcomes on validation data are reported for the full algorithm versus a reduced model (for unknown age and sex) and a further-reduced model (for unknown age, sex, and rhythm history) (CCs = chest compressions, SVM = support vector machine output probability).

Algorithm and Required Input Information	**Defibrillation Success AUC**		**Functional Survival AUC**	
	Without CCs	With CCs	Without CCs	With CCs
Full Model:	0.769	0.740	0.762	0.753
Inputs: *Age, Sex, Prior ROR, SVM*	(0.744-0.771)	(0.711-0.769)	(0.737-0.788)	(0.724-0.781)
Reduced Model (no demographics):	0.774	0.742	0.755	0.750
Inputs: *Prior ROR, SVM*	(0.749-0.799)	(0.713-0.771)	(0.730-0.781)	(0.721-0.778)
Further-Reduced Model (ECG only):	0.748	0.695	0.751	0.746
Inputs: *SVM*	(0.723-0.774)	(0.665-0.726)	(0.726-0.777)	(0.718-0.775)

I. REFERENCES

1. Coult J, Blackwood J, Rea T, Kudenchuk P, Kwok H. A Method to Detect Presence of Chest Compressions During Resuscitation Using Transthoracic Impedance. *IEEE J Biomed Heal Informatics* 2019;[in press]. doi:10.1109/JBHI.2019.2918790.
2. Gong Y, Gao P, Wei L, Dai C, Zhang L, Li Y. An Enhanced Adaptive Filtering Method for Suppressing Cardiopulmonary Resuscitation Artifact. *IEEE Trans Biomed Eng* 2017;64:471–478. doi:10.1109/TBME.2016.2564642.
3. Link MS, Berkow LC, Kudenchuk PJ, Halperin HR, Hess EP, Moitra VK, Neumar RW, O'Neil BJ, Paxton JH, Silvers SM, White RD, Yannopoulos D, Donnino MW. Part 7: Adult Advanced Cardiovascular Life Support. *Circulation* 2015;132:S444–S464. doi:10.1161/CIR.0000000000000261.
4. Johnson B V., Coult J, Fahrenbruch C, Blackwood J, Sherman L, Kudenchuk P, Sayre M, Rea T. Cardiopulmonary resuscitation duty cycle in out-of-hospital cardiac arrest. *Resuscitation* 2015;87:86–90. doi:10.1016/j.resuscitation.2014.11.008.
5. González-Otero DM, Ruiz de Gauna S, Ruiz J, Daya MR, Wik L, Russell JK, Kramer-Johansen J, Eftestøl T, Alonso E, Ayala U. Chest compression rate feedback based on transthoracic impedance. *Resuscitation* 2015;93:82–88. doi:10.1016/j.resuscitation.2015.05.027.
6. Eilevstjønn J, Eftestøl T, Aase SO, Myklebust H, Husøy JH, Steen PA. Feasibility of shock advice analysis during CPR through removal of CPR artefacts from the human ECG. *Resuscitation* 2004;61:131–141. doi:10.1016/j.resuscitation.2003.12.019.
7. Nash MP, Mourad A, Clayton RH, Sutton PM, Bradley CP, Hayward M, Paterson DJ, Taggart P. Evidence for Multiple Mechanisms in Human Ventricular Fibrillation. *Circulation* 2006;114:536–542. doi:10.1161/CIRCULATIONAHA.105.602870.
8. Nanthakumar K, Walcott GP, Melnick S, Rogers JM, Kay MW, Smith WM, Ideker RE, Holman W. Epicardial organization of human ventricular fibrillation. *Hear Rhythm* 2004;1:14–23. doi:10.1016/j.hrthm.2004.01.007.
9. Ten Tusscher KHWJ, Hren R, Panfilov A V. Organization of Ventricular Fibrillation in the Human Heart. *Circ Res* 2007;100:e87-101. doi:10.1161/CIRCRESAHA.107.150730.
10. Weaver WD, Cobb LA, Dennis D, Ray R, Hallstrom AP, Copass MK. Amplitude of

ventricular fibrillation waveform and outcome after cardiac arrest. *Ann Intern Med* 1985;102:53–55.

11. Povoas HP, Bisera J. Electrocardiographic waveform analysis for predicting the success of defibrillation. *Crit Care Med* 2000;28:N210-1.
12. Firoozabadi R, Nakagawa M, Helfenbein ED, Babaeizadeh S. Predicting defibrillation success in sudden cardiac arrest patients. *J Electrocardiol* 2013;46:473–479. doi:10.1016/j.jelectrocard.2013.06.007.
13. Callaway CW, Menegazzi JJ. Waveform analysis of ventricular fibrillation to predict defibrillation. *Curr Opin Crit Care* 2005;11:192–199.
14. Witkowski FX, Leon LJ, Penkoske PA, Giles WR, Spano ML, Ditto WL, Winfree AT. Spatiotemporal evolution of ventricular fibrillation. *Nature* 1998;392:78–82.
15. Gray RA, Pertsov AM, Jalife J. Spatial and temporal organization during cardiac fibrillation. *Nature* 1998;392:75–78.
16. Hastings HM, Evans SJ, Quan W, Chong ML, Nwasokwa O. Nonlinear dynamics in ventricular fibrillation. *Proc Natl Acad Sci U S A* 1996;93:10495–10499.
17. Addison PS. The Illustrated Wavelet Transform Handbook. Taylor & Francis; 2002.
18. Watson JN, Uchaipichat N, Addison PS, Clegg GR, Robertson CE, Eftestol T, Steen P a. Improved prediction of defibrillation success for out-of-hospital VF cardiac arrest using wavelet transform methods. *Resuscitation* 2004;63:269–275. doi:10.1016/j.resuscitation.2004.06.012.
19. Watson JN, Addison PS, Clegg GR, Steen PA, Robertson CE. Practical issues in the evaluation of methods for the prediction of shock outcome success in out-of-hospital cardiac arrest patients. *Resuscitation* 2006;68:51–59. doi:10.1016/j.resuscitation.2005.06.013.
20. Watson JN, Addison PS, Clegg GR, Holzer M, Sterz F, Robertson CE. A novel wavelet transform based analysis reveals hidden structure in ventricular fibrillation. *Resuscitation* 2000;43:121–127.
21. Box MS, Watson JN, Addison PS, Clegg GR, Robertson CE. Shock outcome prediction before and after CPR: a comparative study of manual and automated active compression-decompression CPR. *Resuscitation* 2008;78:265–274. doi:10.1016/j.resuscitation.2008.03.225.

22. Endoh H, Hida S, Oohashi S, Hayashi Y, Kinoshita H, Honda T. Prompt prediction of successful defibrillation from 1-s ventricular fibrillation waveform in patients with out-of-hospital sudden cardiac arrest. *J Anesth* 2011;25:34–41. doi:10.1007/s00540-010-1043-x.
23. Coult J, Blackwood J, Sherman L, Rea TD, Kudenchuk PJ, Kwok H. Ventricular Fibrillation Waveform Analysis During Chest Compressions to Predict Survival From Cardiac Arrest. *Circ Arrhythm Electrophysiol* 2019;12:1–10. doi:10.1161/CIRCEP.118.006924.
24. Shannon CE. A Mathematical Theory of Communication. *Bell Syst Tech J* 1948;27:379–423. doi:10.1002/j.1538-7305.1948.tb01338.x.
25. Rosso OA, Blanco S, Yordanova J, Kolev V, Figliola A, Schürmann M, Başar E. Wavelet entropy: a new tool for analysis of short duration brain electrical signals. *J Neurosci Methods* 2001;105:65–75. doi:10.1016/S0165-0270(00)00356-3.
26. Nunes RR, Almeida MP de, Sleigh JW. Spectral Entropy: A New Method for Anesthetic Adequacy. *Rev Bras Anestesiol* 2004;54:404–422. doi:10.1590/S0034-70942004000300013.
27. Lever NA, Newall EG, Larsen PD. Differences in the characteristics of induced and spontaneous episodes of ventricular fibrillation. *EP Eur* 2007;9:1054–1058. doi:10.1093/europace/eum194.
28. Pincus SM. Approximate entropy as a measure of system complexity. *Proc Natl Acad Sci U S A* 1991;88:2297–2301. doi:10.1073/pnas.88.6.2297.
29. Lin L-Y, Lo M-T, Ko PC-I, Lin C, Chiang W-C, Liu Y-B, Hu K, Lin J-L, Chen W-J, Ma MH-M. Detrended fluctuation analysis predicts successful defibrillation for out-of-hospital ventricular fibrillation cardiac arrest. *Resuscitation* 2010;81:297–301. doi:10.1016/j.resuscitation.2009.12.003.
30. Chicote B, Irusta U, Alcaraz R, Rieta J, Aramendi E, Isasi I, Alonso D, Ibarguren K. Application of Entropy-Based Features to Predict Defibrillation Outcome in Cardiac Arrest. *Entropy* 2016;18:313. doi:10.3390/e18090313.
31. Chicote B, Irusta U, Aramendi E, Alcaraz R, Rieta J, Isasi I, Alonso D, Baqueriza M, Ibarguren K. Fuzzy and Sample Entropies as Predictors of Patient Survival Using Short Ventricular Fibrillation Recordings during out of Hospital Cardiac Arrest. *Entropy* 2018;20:591. doi:10.3390/e20080591.

32. Watson JN, Addison PS, Clegg GR, Steen PA, Robertson CE. Wavelet transform-based prediction of the likelihood of successful defibrillation for patients exhibiting ventricular fibrillation. *Meas Sci Technol* 2005;16:L1–L6. doi:10.1088/0957-0233/16/10/L01.
33. Shandilya S, Ward K, Kurz M, Najarian K. Non-linear dynamical signal characterization for prediction of defibrillation success through machine learning. *BMC Med Inform Decis Mak* 2012;12:116. doi:10.1186/1472-6947-12-116.
34. Foomany FH, Umapathy K, Sugavaneswaran L, Krishnan S, Masse S, Farid T, Nair K, Dorian P, Nanthakumar K. Wavelet-based markers of ventricular fibrillation in optimizing human cardiac resuscitation. 2010 Annu Int Conf IEEE Eng Med Biol, IEEE; 2010, p. 2001–2004. doi:10.1109/IEMBS.2010.5627841.
35. Brown C, Dzwonczyk R. Estimating the duration of ventricular fibrillation. *Ann Emerg Med* 1989;18:1181–1185.
36. Eftestøl T, Sunde K, Ole Aase S, Husøy JH, Steen PA. Predicting Outcome of Defibrillation by Spectral Characterization and Nonparametric Classification of Ventricular Fibrillation in Patients With Out-of-Hospital Cardiac Arrest. *Circulation* 2000;102:1523–1529. doi:10.1161/01.CIR.102.13.1523.
37. Brown CG, Dzwonczyk R. Signal analysis of the human electrocardiogram during ventricular fibrillation: frequency and amplitude parameters as predictors of successful countershock. *Ann Emerg Med* 1996;27:184–188.
38. Alpaydin E. Introduction to Machine Learning. 3rd ed. MIT Press; 2014.
39. James G, Witten D, Hastie T, Tibshirani R. An Introduction to Statistical Learning. vol. 103. New York, NY: Springer New York; 2013. doi:10.1007/978-1-4614-7138-7.
40. Howe A, Escalona OJ, Di Maio R, Massot B, Cromie N a, Darragh KM, Adgey J, McEneaney DJ. A support vector machine for predicting defibrillation outcomes from waveform metrics. *Resuscitation* 2014;85:343–349. doi:10.1016/j.resuscitation.2013.11.021.
41. He M, Gong Y, Li Y, Mauri T, Fumagalli F, Bozzola M, Cesana G, Latini R, Pesenti A, Ristagno G. Combining multiple ECG features does not improve prediction of defibrillation outcome compared to single features in a large population of out-of-hospital cardiac arrests. *Crit Care* 2015;19:425. doi:10.1186/s13054-015-1142-z.
42. Platt JC. Probabilistic Outputs for Support Vector Machines and Comparisons to

Regularized Likelihood Methods. *Adv Large Margin Classif* 1999;10:61–74.

43. Reed MJ, Clegg GR, Robertson CE. Analysing the ventricular fibrillation waveform. *Resuscitation* 2003;57:11–20. doi:10.1016/S0300-9572(02)00441-0.
44. Martin DR, Brown CG, Dzwonczyk R. Frequency analysis of the human and swine electrocardiogram during ventricular fibrillation. *Resuscitation* 1991;22:85–91. doi:10.1016/0300-9572(91)90067-9.
45. Jalife J. Ventricular Fibrillation: Mechanisms of Initiation and Maintenance. *Annu Rev Physiol* 2000;62:25–50. doi:10.1146/annurev.physiol.62.1.25.
46. Eftestøl T, Sunde K, Aase SO, Husøy JH, Steen P a. "Probability of successful defibrillation" as a monitor during CPR in out-of-hospital cardiac arrested patients. *Resuscitation* 2001;48:245–254.
47. Neurauter A, Eftestøl T, Kramer-Johansen J, Abella BS, Sunde K, Wenzel V, Lindner KH, Eilevstjønn J, Myklebust H, Steen PA, Strohmenger H-U. Prediction of countershock success using single features from multiple ventricular fibrillation frequency bands and feature combinations using neural networks. *Resuscitation* 2007;73:253–263. doi:10.1016/j.resuscitation.2006.10.002.